DISSERTATION

THE REDUCTION OF PARTICULATE MATTER EMISSION RELEASED DURING PYROLYSIS AND IGNITION OF THERMALLY THICK WOOD

Submitted by

John Joseph Flynn

Department of Mechanical Engineering

In partial fulfillment of the requirements

For the Degree of Doctor of Philosophy

Colorado State University

Fort Collins, Colorado

Spring 2026

Doctoral Committee:

Advisor: Tami C. Bond

Shantanu Jathar
Bret Windom
Jeffery Pierce

ABSTRACT

THE REDUCTION OF PARTICULATE MATTER EMISSION RELEASED DURING PYROLYSIS AND IGNITION OF THERMALLY THICK WOOD

Solid fuels in the indoor home environment are used in day-to-day life by nearly a third of the entire global population. Consequently, exposure to household air pollution from wood burning results in millions of years of lost life, annually. Emission of organic particulate matter with a diameter less than 2.5 μm ($PM_{2.5}$) is released in the process of burning, especially prior to ignition. Efforts to reduce $PM_{2.5}$ through improved cook stoves have made some progress, however exposure limits still well exceed the threshold set by the World Health Organization.

While improving cook stove technology can be beneficial to achieving lower emission rates, a less common approach to the reduction of $PM_{2.5}$ is the use of wood burning fundamentals. Developing new methods of burning is an under-utilized approach to reduce organic $PM_{2.5}$ from wood combustion. Emission reductions derived from quick ignition and formation of a flame may aid in reducing $PM_{2.5}$ exposure rates.

This dissertation reports findings from the application of ignition theory developed by the field of fire safety engineering to the ignition of wood as a method of reducing $PM_{2.5}$. Four objectives are addressed including (1) identify necessary language and frameworks to communicate needs from the cook stoves research field to fire science engineers for reducing PM pollution, (2) experimentally isolate limiting factors for controlling ignition that aims to reduce energy demand and PM release, (3) experimentally characterize pre-ignition PM release associated with ignition limitation factors, and (4) identify guidelines for ideal burning using ignition and PM

release factors identified from experimentation to provide recommendations for exposure reduction.

This work couples heat and mass transfer principles with aerosol sampling methodologies to identify burning mechanisms required for deliberate ignition of wood. Experiments were performed that leverage the anisotropic heat and mass transfer properties of wood in a series of pyrolysis and ignition trials. Results were used to identify a previously unidentified ignition factor called pyrolytic acceleration. A metric called Ignition Energy Ratio was defined to quantify energy demands associated with wood grain direction, heat flux, and wood type. Particle measurements were used to identify a new burning mechanism involving reactions which produce particulate matter before pyrolytic acceleration occurs. Lastly, results were compiled to provide guidance for stove designers and developers of wood burning protocol based on findings. In conclusion, this dissertation reports on the use of fire science principles for the reduction of $PM_{2.5}$ and establishes a link between previously unaffiliated fields of research.

ACKNOWLEDGEMENTS

This work would not be possible without the incredible support and guidance from so many amazing people in my life. While it is not possible to identify every person who has impacted my quality of life during the extent of this work, I would like to acknowledge a few special people and groups.

Thank you to my advisor, Tami, who has done so much for me to ensure my success. Her endless support and unworldly patience through the good times and bad made a world of difference to me. Thank you, Tami, for challenging and enabling me to reach further than I thought was possible.

I want to acknowledge my amazing collaborators David Morrisset and Rory Hadden, who brought a new level of excitement to this "science" work. Thank you for the good laughs and the boundless inspiration for this research.

Thank you to my friends for so many side-splitting laughs and incredible adventures which served to enrich the grad school experience in a way that makes me feel so blessed. I feel grateful for so many people. A special thanks to my friends from the Fall 2020 cohort; Abe Dearden, Ben Platt, Dylan Giardina, Robi Vercellino, and Brye Windell.

I want to acknowledge my yoga community and my amazing neighbors. A special thanks to my yoga peeps Maj-Lis Delgado, Jana and Ben Stratton, Brad Hoback, Will Bromley, Jacob and Rebecca Michel, and Miles Knight. And a special thanks to my neighbors who have become family; Tom and Barb, Sonny, Stacy, Ana, Viv, Julia, and Sam.

Finally, and most importantly, thank you to my parents Tom and Beth, my sisters Alexandria and Leslie, my brother-in-law Chris, and my nephews Flynn and Jack. The strong feelings of support and love you all provide are enough to make me feel like I can do anything. I love you all.

TABLE OF CONTENTS

LIST OF TABLES

LIST OF FIGURES

Chapter 1

Introduction

An estimated 2.6 billion people (2.2 – 3.1 billion[1]) globally lack access to clean cooking fuels [1]. Without clean cooking stoves the exposure of pollutants released from alternative fuel sources, like wood, results in adverse health effects. This exposure means that household air pollution from solid fuels ranks as the third highest individual health risk for men and women combined, globally [2]. Global emission inventories show that 20% of black carbon and organic carbon aerosol emissions to the atmosphere are attributable to domestic combustion of solid fuels [3].

Efforts that have been made to improve the quality of common stoves include the installation of liquid petroleum gas (LPG) or natural gas cooking units where possible, distribution of clean-burning cook stoves, and the design of new stoves that more efficiently burn wood. While these approaches serve to improve upon the emissions from some wood-fired stoves during consistent operation, the widespread use of wood fuel persists with little measurable improvement. This continued use demands more thorough investigation of how to burn wood with minimized particulate matter release. The present dissertation involves the combined use of aerosol science and fire science to address the problem of $PM_{2.5}$ exposure.

[1] Confidence interval of 59-71 percent

This investigation employs principles developed by fire safety engineers for the opposite purpose of their original conception: whereas fire safety engineering aims to prevent inadvertent ignition, the purpose of this work is to optimize deliberate ignition. The naturally occurring properties of wood are leveraged in a way that requires no sophisticated technology and yields information on burning conditions that can be utilized for reduction of PM. Some complications arise from the type of wood used in real-world fire settings. In this work we use laboratory prepared wood samples to avoid confounding factors like bark, knots, sap, and cracks ubiquitous in harvested wood fuel. While these features may cause ignition to happen faster or slower this work aims to derive findings from the anisotropic structure of the wood grain through the application of fire safety engineering fundamentals. This work presents findings which are transferable to real-world wood despite the use of laboratory curated samples.

This dissertation is situated at the intersection of fire science and aerosol science. Fire science has a particular focus on the 'bottom-up' thermal and physical mechanics involved with pyrolysis, ignition, and combustion. Significantly less effort is dedicated to the release of condensable tars that form particulate matter, which in fire science are generally classified as emission products with high molecular weight and often referred to generally as the 'gas phase' or 'pyrolyzates.' Conversely, the field of atmospheric aerosols addresses the appearance of particulate matter released from wood burning in the atmosphere with less focus on the mechanisms involved with the source release. The distinct difference between disciplines results in a knowledge gap situated in the region of particulate matter release and burning mechanisms.

Minimal work is reported at the intersection of aerosol science and fire science. This project serves to link the 'bottom-up' mechanisms from fire science to the 'top-down' knowledge of $PM_{2.5}$ release and the ill effects on human health. The focus of this body of work is to reduce the release

of $PM_{2.5}$ by identifying the conditions that lead to fast ignition and conversion of pyrolysis products to CO_2 and water by the occurrence of ignition and combustion. This is accomplished by situating experimental investigation in the space that connects these two fields. By employing fire science fundamentals to achieve optimized ignition and using aerosol science concepts to assess improvements in reduced PM emission a more rigorous understanding of the transition from wood burning to $PM_{2.5}$ release to ignition will be accomplished.

Chapter 2

Literature review

A significant amount of work has been done towards understanding nuanced aspects of exposure to particulate matter with diameters below ≤ 2.5 μm ($PM_{2.5}$) in a cooking environment [4–8]. Exposure studies indicate how $PM_{2.5}$ inhalation occurs for vulnerable groups in the indoor environment [9,10]. Women and children are identified as especially high risk to elevated PM exposure due to their predominant social roles in preparing food in most cultures [2,11]. This higher exposure is compounded by other challenges like limited availability of wood and other burnable biomass which results in the use of more polluting fire-starter materials like plastic [12,13].

The need to reduce the amount of fuel required to accomplish cooking tasks has resulted in technological improvements for burning wood. The term “improved cook stoves” is used to describe cook stove technologies which aim to improve stove performance through metrics that include heat output, reduced fuel consumption, and lower harmful emissions. In the context of reducing household air pollution there appears to be little consensus that improved cook stoves reduce $PM_{2.5}$ exposure. Reports indicate marginal improvements, but they do not achieve levels which can be considered “improved” by World Health Organization exposure standards [14–17].

2.1 Start-up in wood stoves

The importance of small-scale combustion sources for the atmosphere has led to many measurements that characterize emission performance [13,18–24]. Decades of cook stove design research have significantly improved the emissions produced by solid-fuel combustion [4]. Improved cook stoves have reduced emissions by 50 % in some cases [18,20]. However, Roden *et al.* identified that analysis of improvements in cook stove performance contained a discrepancy between laboratory and field measurements [13,19,21]. These studies found that improved cook stoves do reduce emissions, but those improvements occur more often during high temperature, steady operation.

Chen *et al.* [25] assessed time-resolved data from field and laboratory situations to determine the causes of discrepancy. Figure 1 shows that in-use burning produces more light-colored particles at low combustion efficiency than standardized laboratory tests. It also shows that periods of high emission (large instantaneous emission factor) contribute about half the total emitted particulate matter. These conditions often occur during initiation of combustion, or 'start-up.' This discrepancy may not appear in laboratory measurements because start-up is excluded or liquid fire-starters are used. In the language of the cook stove community 'start-up' refers to the transfer of heat to wood in a cold fire box that causes the wood to ignite and burn. A stove user needs to collect material to accomplish this phase in addition to collecting necessary fuel.

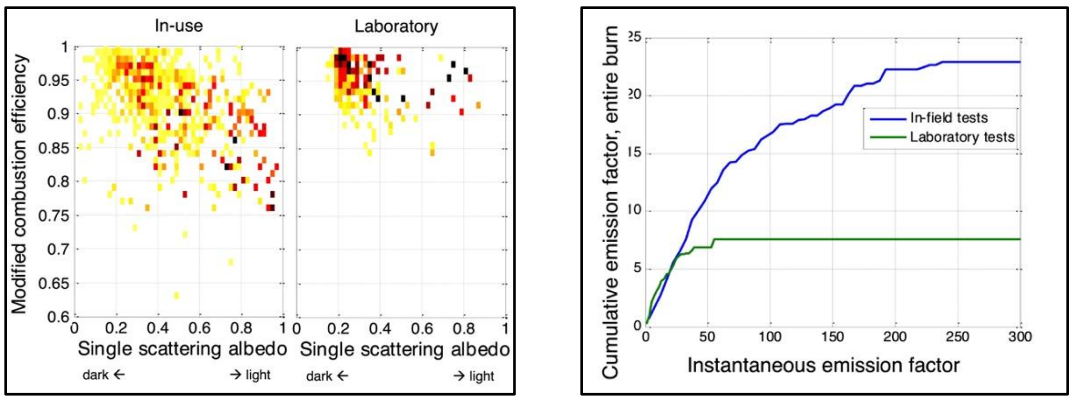

Figure 1. Time-resolved data show differences in laboratory and field performance of improved stoves. Left two panels: In-use stoves emit more light-colored particles at low combustion efficiency. Right panel: More than half the total emission for the entire burn occurs during periods when emissions per mass of burned fuel are high. Emission factors are determined from ratio between light scattering (approximately proportional to particulate matter concentration) and gaseous carbon. Modified from Chen *et al.*, 2012, Figures 3 and 5 [25].

These observations raise the following question: Do we know ways to quickly ignite wood in a cold-fire box?

2.2 Perspectives from aerosol science

Domestic wood combustion is studied in the science of atmospheric aerosols, as it produces emissions that affect human health [9,26–29]. Chemical characterization [30–33], secondary organic aerosol formation and particle partitioning [34–40], and technology improvements [18–21,41] are common topics studied in aerosol sciences relevant to wood combustion. The aerosol science field employs measurement devices and predictive modelling to characterize the nature of the PM exposure and toxicity of inhaled constituents. Coordination of aerosol sampling with epidemiology has improved understanding of comorbidities linked to chronic exposure [5,42,43]. However, attributing mechanisms of particulate matter formation to solutions for reducing exposure is not common in the aerosol science field. In other words, PM becomes a pollutant of interest in most of the works mentioned only after it is ejected from a burning piece of fuel.

A small number of studies link the formation of PM with discussion of fire physics [44,45], but this practice is less common. More common is the literature regarding the mechanisms of particulate matter formation arising after thermal conversion of wood and biomass combustion. Some specific reviews on this topic include those contributed by Reid [46], Ning [47], Obaidullah [48], and Chen [49]. These reviews thoroughly characterize the chemical signature of PM forming molecules, nucleation mechanisms, particle morphology, particle size distributions, and factors that affect these properties. After classifying the formation mechanisms and particle properties, additional focus is given to the fate of these particles in the atmosphere or indoor air environment. Descriptions of the release of particle-forming volatiles correlated to specific burning mechanisms are not discussed.

Methods of reducing organic PM by an ignition event are seldom mentioned, although substantial reductions have been observed. Haslett *et al.* show an approximately 90 % drop in the ratio of organic aerosol to total aerosol after ignition occurs [45]. Elsasser *et al.* report an 80 % decrease in organic matter released after ignition (see Figure 2) [50]. Other works emphasize that the majority of organic $PM_{2.5}$ is released before ignition [8,51]. For the most part, atmospheric studies classify combustion types into only “flaming” and “smoldering” or categorize emission factors by situation [46]. Emissions are perceived as highly variable or stochastic.

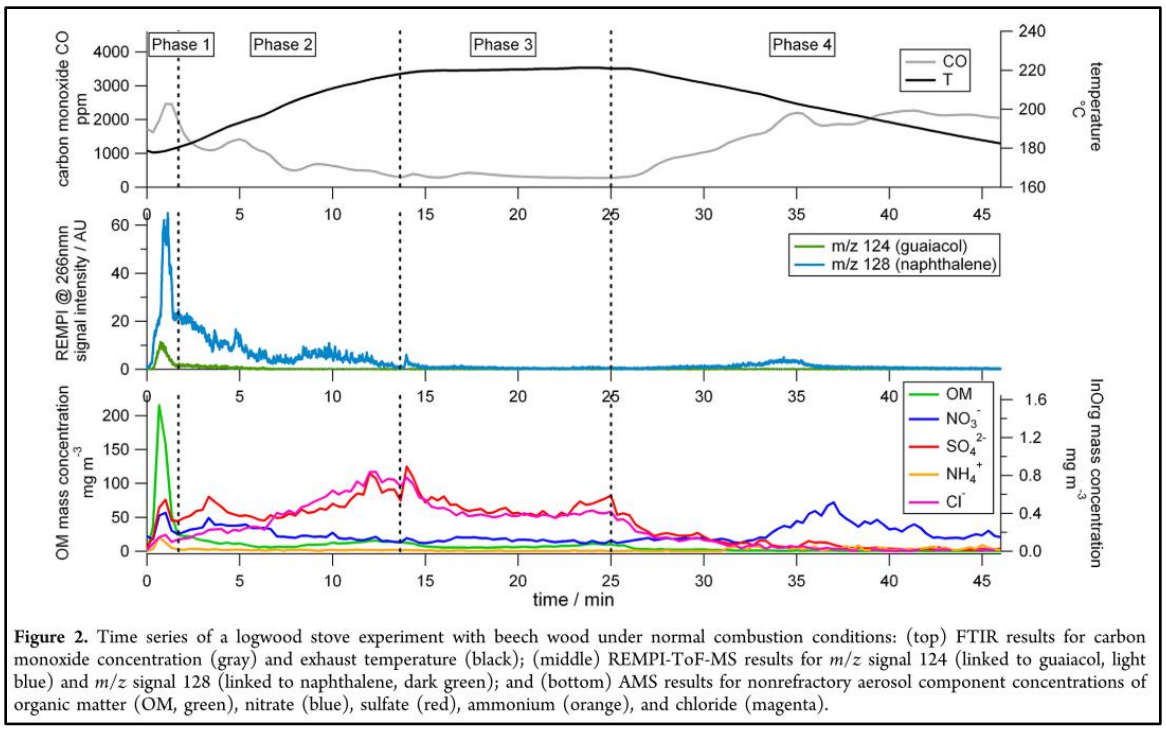

Figure 2. Time series of a logwood stove experiment with beech wood under normal combustion conditions: (top) FTIR results for carbon monoxide concentration (gray) and exhaust temperature (black); (middle) REMPI-ToF-MS results for m/z signal 124 (linked to guaiacol, light blue) and m/z signal 128 (linked to naphthalene, dark green); and (bottom) AMS results for nonrefractory aerosol component concentrations of organic matter (OM, green), nitrate (blue), sulfate (red), ammonium (orange), and chloride (magenta).

Figure 2. A figure extracted from Elsasser *et al.* [50] showing the signal response of organic matter concentration (green, bottom panel) after the ignition event.

2.3 Perspectives from fire science

In contrast to the perception within atmospheric science, Fawaz *et al.* showed that mass release from burning of biomass is highly predictable [44,52,53]. They utilized a two-dimensional predictive model (Gpyro) and were able to reproduce experiments. In these works authors identified the need to focus efforts to the transient ignition phase for reducing PM exposure.

The difference between the aerosol-science communities and the fire-science communities is the emphasis on principles of mass and heat transfer as they describe pyrolyzing wood. In fact, the circumstances for ignition to occur are thoroughly described in the fire science literature [54–58]. Fuel products released from wood during pre-ignition pyrolysis notably include CO, CO_2, and a large array of heavier organic species [31] which in this work are generalized as “wood tars.” Condensation of volatilized wood tar causes the formation of particulate matter prior to wood

ignition [59]. A significant factor in reducing this tarry particulate matter is the presence of a flame, initiated by an ignition event. Ignition occurs when the ratio of heat 'in' from an external source creates a mass flux of fuel 'out' which is sufficient to support ignition and a sustained flame for a specific heat flux. This minimum criteria for flame stability suggests that a fast transition from endothermic pyrolysis to exothermic combustion is possible if an ignition supporting ratio of heat to fuel can be achieved.

2.3.1 Pre-ignition pyrolysis and release of PM-forming mass

Bartlett *et al.* describes the process of starting a fire which begins with application of heat to the wood followed by a rise in surface temperature which eventually initiates pyrolysis of the solid material [60]. Pyrolysis is defined as "the chemical degradation of a substance by the action of heat" [55]. This chemical degradation of a substance causes the release of pyrolysis products, some of which condense to form aerosol droplets.

During this stage of pre-ignition pyrolysis a quantity of wood is converted from the solid matrix to a polluting gaseous mixture; broadly called 'smoke' in lay-terms. Fawaz reports that after pyrolysis at temperatures between 400 °C to 600 °C the solid char remaining ranges from 18 % to 30 % of the initial mass [52]. The other 70 % to 82 % of the initial mass is converted to pyrolysis products. Hydrocarbons released during pyrolysis range in molecular weights. Low molecular weight pyrolysis products, like methane, have high volatility causing them to reside in the gas phase after formation [61]. As molecular weight increases, pyrolysis products generally decrease in volatility. The liquefaction of lower volatile organic compounds (VOCs) form a 'condensed phase' droplet, referred to as 'particulate matter' or 'aerosol particles.'

The endothermic formation of particulate matter (PM) will occur if a high enough heat flux is applied to the surface of a piece of wood. The minimum surface temperature which results in mass loss is 200 °C [60]. A "critical heat flux" is required for the possibility of ignition to occur and begins around 10 kW to 13 kW during piloted ignition and 25 kW to 33 kW for auto ignition cases [60]. Ignition marks a transition from endothermic pyrolysis to exothermic combustion. As a result of this transition to exothermic chemistry, VOCs released during pyrolysis are converted from PM-forming tars to light weight combustion products like CO_2 and water, which remain in the gas phase. Pyrolysis products will not escape the burning process to form particulate matter so long as they pass through a flame. Therefore, particulate matter can be reduced by accomplishing 'deliberate ignition.'

2.3.2 Chemistry of wood ignition

Ultimately, the goal is to achieve a stable and sustained flame through which all emissions passes. This entails the solid fuel producing a stochiometric balance of combustible products which results in constant flame feedback radiation. Fire science and fire safety engineering has referred in the past to this stoichiometric balance of fuel as the *critical mass flux* (CMF) [62–64]. While this metric has fallen out of use in favor of the critical heat flux, it represents the necessary balance between incident heat on the sample which results in the conversion of solid wood to a combustible fuel which supports equilibrium for sustained burning. Limiting factors for CMF include heat flux in and mass flux out, as well as fuel properties, heat of pyrolysis, oxygen mixing, and heat losses to the surrounding. CMF is no longer a preferred metric due to its dependency on fuel and burning conditions [59,65], its experimental ambiguity [58], and the difficulty of integrating CMF in models [65–67].

A key factor in the application of fire science to the ignition of solid fuels is the dependence on the transport phenomena of heat and mass. This represents a distinct approach from combustion physics, in which chemical mechanisms and kinetics of fuel oxidation are preferred descriptions for physical processes. The use of heat and mass transfer frameworks in fire science reflects the complexity of the fuel types encountered. As such, a global heat of reaction is generally considered sufficient rather than resolving the heat of reaction of each constituent species undergoing combustion. Understanding the species produced through the sequence of dehydration, devolatilization of non-fuel bound species, and charring further informs this framework.

Combustion chemistry plays a secondary role in many ignition prediction methods in fire science; however, related physical properties, like fuel volatility, play a significant role in understanding the formation of aerosolized particulate matter. The general chemical mechanisms associated with the ignition event therefore provide important context. Wood is a complex solid matrix of three main structural, polymeric material types; cellulose, hemi-cellulose, and lignin [68]. These polymeric structures are comprised of five "wood sugar" monomers which are glucose, mannose, galactose, arabinose, and xylose [69]. Fuel-bound functional groups like alcohols and acids are present in high concentrations.

Broadly, products resulting from pre-ignition pyrolysis are summarized as char, tar, and gases [70]. Mass spectroscopy of wood emissions has identified the primary gaseous fuel constituents released as wood surface temperatures increase. Avery, et al. conducted pyrolysis experiments at 400 °C, 500 °C, and 600 °C while utilizing Aerosol Mass Spectroscopy (AMS) analysis to determine which chemical species are released during pyrolysis [31]. At low temperatures gases released are "primary wood components" like wood sugars, while increasing temperature decreases H/C ratios [31]. During the initial heating of wood the first mass release

occurs due to dehydration at 100 °C. As heating continues surface temperatures ranging from 150 °C to 300 °C produce oxygenated products including acetic acid, formic acid, CO, and CO_2 [68]. As temperatures increase to 250 °C – 350 °C cellulose depolymerization and fragmentation reactions occur which broaden the diversity of species released [71]. From these reactions radical species including H^+, O^{2-}, and OH^- are generated which aid in the initiation of chain-branching reaction mechanisms required for ignition and sustained combustion [68,72].

2.3.3 Deliberate Ignition

The decades of literature established by the fire science and fire safety engineering communities can aid in understanding deliberate ignition of wood. A founding father in the field, H.W. Emmons, describes 'fire science' as the "understanding of fire through the methods of science" [73]. This fairly unhelpful description is supplemented here insomuch that the field of fire science relies less on the kinetics and reaction pathways favored by the combustion physics community and more on heat and mass transfer phenomena used to describe fire behavior. 'Fire safety' or 'fire safety engineering' refers to the application of fire science to the protection of human life and property [59]. The development of wood burning and wood ignition concepts and theory used today were established in the field of fire science by Spalding [74,75] and Emmons [76] followed by a large effort in applied theory and experimentation contributed by Rasbash [77,78], Drysdale [56,79], Tewarson & Pion [80–83], Janssens [84–86], Spearpoint [87] and Quintiere [88]. Mathematical modeling and derivations have been contributed by these authors with further contributions by the groups of Fernandez-Pello [67,89,90] and Di Blasi [70,91,92].

Comprehensive reviews of ignition criteria and fire science involved with burning thermally thick wood include works by Atreya [54], Drysdale [56,59], Janssens [93], Babrauskas

[58], Torero [57], and Bartlett [60]. While these works include thorough details concerning the ignition and combustion of solid wood, it is important to note that these developments were largely intended for application in the prevention of ignition through fire safety engineering. There is no discernable application to the deliberate ignition of wood by these authors. Very few descriptions are provided in these texts on the generation of particulate matter, with rare acknowledgements that pyrolysis products will cause the formation of condensed phase particles. Drysdale provides significant detail regarding aerosol formation including a description of condensing tars and the chemical pathway to form soot [59].

As a final matter for building context, there is a subtle emphasis in the fire science literature on the role of anisotropic heat and mass transfer during pyrolysis and ignition which is applied in this work to the release of PM and the conversion of PM to lightweight gas by the creation of a flame. To accomplish this union of concepts, it is important to understand the heat and mass transfer properties of wood. The presence of grain structures which transport water through a living tree cause directionally-dependent (anisotropic) heat and mass transfer to occur when wood is burning. Figure 3 shows the directionality of wood grain, referred to as the longitudinal direction, the radial direction, and the tangential direction. Thermal conductivity has been shown to be 1.5 to 3 times greater in the longitudinal direction compared to that of the radial and tangential directions [94–96]. This is caused by the directionality of the grain structure, which incidentally affects not only heat transfer but the resistance to mass release as well.

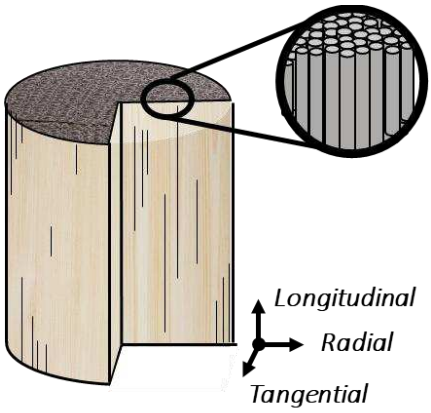

Figure 3. Wood directional coordinate system for hardwood. Vessel structures shown, expanded.

Woods are classified as hardwood and softwood. Hardwoods are identified by having the anatomical feature of vessel structures which are used to transport water in a living hardwood tree. Vessels are tubular structures which run in the longitudinal direction of the wood grain and allow for long distance water transport (shown in Figure 3). Softwoods are characterized by the presence of cellular structures called tracheids which are linked by small orifices called pits. The long-distance transport of mass in softwoods is limited by mass transfer occurring from tracheid to tracheid through these intercellular pits. Hardwoods have higher permeability in the longitudinal direction which serves to increase the rate of heat transfer as well as decrease resistance to mass transfer. In this study, the anisotropic features present in both wood types are used to modify heat and mass transfer.

2.4 Summary

This chapter provides an overview of several relevant topics which provide background context to the uninitiated reader. The benefits and deficiencies of improved cook stoves were discussed in section 2.1. Perspectives on ignition in a cold stove from an aerosol science

perspective were described in section 2.2. The pre-ignition pyrolysis of wood and release of PM-forming emissions were discussed in section 2.3 along with the concept of deliberate ignition.

The next chapter outlines research objectives in this dissertation and introduces the three chapters that follow in which solutions to the proposed objectives are discussed.

Chapter 3

Research objectives

This work has four objectives that aim to use experimental techniques to identify causes of PM release, solutions for preventing exposure, and methods of communicating findings.

3.1 Objective 1: Identify necessary language and frameworks to communicate needs from the cook stoves research field to fire science engineers for reducing PM pollution.

This objective aims to create language and conceptual frameworks to aid in mapping cook stove research needs to the field of fire science. The required fundamentals to solve problems related to ignition and PM reduction exist but are situated in different scientific fields. The purpose of this objective is to develop language and frameworks that inform an uninitiated community why PM reduction is important and identify gaps that need addressed. Tasks in this objective also relate to identifying the necessary fire science principles required to solve PM exposure problems. This effort can aid in the creation of a research space that combines principles from fire safety engineering and aerosol science to solve problems that receive minimal attention from either field. The work supporting this objective is reported in Chapter 4 and Chapter 6.

3.2 Objective 2: Experimentally isolate limiting factors for controlling ignition that aims to reduce energy demand and PM release.

This objective aims to utilize fire science fundamentals to characterize factors that reduce energy requirements for ignition and reduce PM release. Tasks required for this objective involve investigation of ignition and pyrolysis that leverage the material characteristics of wood. More specifically, this objective requires the design and execution of a campaign of experiments which in combination isolate the effects of material properties, heating conditions, and flammability. Experiments will be used to identify limiting factors that control ignition and pre-ignition release of PM. Factors available to a stove user will be identified. Findings from this study are presented in Chapter 4 and Chapter 6.

3.3 Objective 3: Experimentally characterize pre-ignition PM release associated with ignition limitation factors.

This objective aims to utilize particle measurements in combination with fire science experimentation to investigate PM release related to ignition. This objective requires identification of factors driving the release of PM and how those factors relate to controlling ignition. Tasks for this objective require the design and execution of a series of tests that combine fire science experiments with aerosol sampling methods. Focus will concentrate on the characterization of aerosol release during the pre-ignition stage of burning. Coordination of ignition limitations to PM release will aid in identifying the role that PM plays in achieving ignition. The work supporting this objective is discussed in Chapter 5.

3.4 Objective 4: Identify guidelines for ideal burning using ignition and PM release factors identified from experimentation to provide recommendations for exposure reduction.

This objective aims to condense findings from experimentation for dissemination to stove designers and developers of burning protocol. Necessary burning fundamentals and PM release factors will be combined with language and communication frameworks needed to inform future work performed by stove and fire science researchers. Additional emphasis will be placed on connecting findings to needs of stove users. Tasks for this objective involve the collection of lessons learned from experimentation to describe ideal burning scenarios which reduce energy consumption and PM release. The work supporting this objective is discussed in Chapter 6.

Chapter 4

Exploiting wood species and grain orientation to illuminate the onset of pyrolysis and ignition in deliberate combustion

This Chapter contains material submitted to the journal Fuel [97]. Co-authors include John J. Flynn, David Morrisset, Rory M. Hadden, Tami C. Bond. My contributions were Conceptualization, Investigation, Data curation, Data analysis, Writing – original draft

4.1 Introduction

Wood plays an important role as a biomass feedstock to provide energy to cook and heat for billions of people who lack access to modern energy sources [7]. These individuals are vulnerable to high exposures of particulate matter and other products of incomplete combustion; respiratory and other ailments attributable to these exposures result in millions of years of lost life [2]. Particulate matter from combustion typically has diameters below 2.5 microns ($PM_{2.5}$), a size that is commonly associated with health effects. Minimizing the health hazards posed by the use of woody biomass as a fuel requires both social and technological approaches.

Solid-fuel burners (e.g., wood burning cook stoves) typically require introduction of virgin fuel during operation which must undergo pyrolysis before it can ignite. Measurements of in-use combustion have shown that substantial fractions of $PM_{2.5}$ emission, and thus exposure, occur while solid fuels are pyrolyzing prior to flaming ignition [25,98]. PM release can happen to freshly added fuel even if ignition and sustained flaming of other fuel in the firebox has occurred. In the deliberate combustion of biomass, ignition is advantageous, as it reduces PM emissions and

increases the system efficiency. Features of the system – the location of virgin wood in the combustion chamber, as well as its size, quantity and origin – all affect the mass of pyrolyzate generated and whether or not these products ignite and undergo gas-phase oxidation. Pyrolyzate is defined here as unburned fuel products including gases from incomplete combustion (e.g., CO) and condensed tar appearing as aerosolized particles.

Empirical work on improving solid-fuel devices to reduce human exposure generally neglects the pre-ignition pyrolysis and ignition phases of wood combustion [99,100]. The aim of the present work is to describe the factors that affect ignition of woody biomass as a prelude to minimize emission of aerosol pyrolysis products. We rely on experiments previously reported in fire safety and fire science, but we emphasize a different application: making these principles useful for "stove design," or practical design of deliberate combustion devices. In order to be useful to the stove design community, a model of deliberate combustion would identify the main variables that characterize the overall process [101]. The model must not rely on a large number of input parameters that are unknown, or that can be determined only by measurements of an identical situation, which would render the model ineffective for practical application. Therefore, our efforts here are directed to determining the factors that affect the production of pyrolyzate for prolonged periods before ignition.

4.2 Background

4.2.1 Phases of Wood Burning

Figure 4 shows the connection between phases of woody fuel burning and smoke release in the context of deliberate combustion. Here we use the term smoke, a lay term for pyrolyzate, generically to include products of pyrolysis as well as products of gas-phase combustion. Phase I

represents heating of the material up to the onset of pyrolysis. Phase II is characterized by increase in the mass loss rate as pyrolysis begins, gas phase ignition (provided the pyrolysis products are generated at a sufficient rate to form a flammable mixture at the location of a pilot) and transient burning. Gas-phase oxidation reactions consume pyrolysis products and produce carbon dioxide; they also increase heat flux to the solid fuel [102]. Phase III is a quasi-steady period of burning after the formation of a char layer [103], and Phase IV is the decay in burning rate as the combustion transitions to smouldering or surface oxidation [88]. The majority of emitted particulate matter is unburned pyrolyzate, known as "organic carbon" in the atmospheric community, rather than the elemental carbon-based "soot" formed in flames [12,13]. Fawaz *et al.* confirmed that mass loss attributed to thermal degradation (pyrolysis) is relevant to $PM_{2.5}$ and exposure, as particulate matter release was proportional to mass loss rate throughout burning [53] and remained chemically constant as determined by Aerosol Mass Spectroscopy [31].

In this work we are interested in determining the factors which affect transition from release of PM during Phase I to flaming combustion of PM during Phase II. Since governing factors and practical outcomes differ for each phase; the work reported here emphasizes Phase I. During Phase 1 stove users commonly deplete fire-starting resources to accomplish ignition. Consequently. factors to consider include achieving ignition of thermally thick fuel with limited tinder and kindling resources [11].

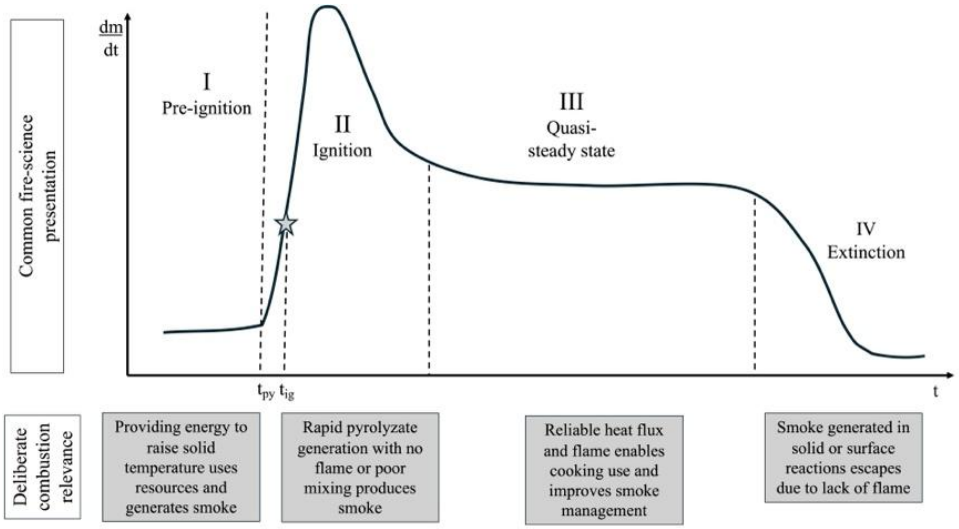

Figure 4. Phases of solid combustion identified in fire science literature and their relevance to deliberate combustion and smoke release. Labels tpy and tig on the x-axis refer to the conventional onset of pyrolysis and of ignition, respectively.

4.2.2 Time to Ignition Theory

Most theories treat a time to ignition as a relevant measure; a simple relationship for time to onset has been derived by assuming that the reaction accelerates when the surface temperature reaches a critical temperature T_s [57,87,105,106]:

$$t_{onset} = \frac{\pi k_s \rho_s c_s (T_s - T_o)^2}{4\left(\dot{q}_e{}''\right)^2} \quad (1)$$

The onset time t_{onset} itself refers to either the beginning of pyrolysis (t_{py}) or ignition (t_{ig}), with the former being slightly shorter than the latter [107]. In this equation, k_s is thermal conductivity, ρ_s is density, c_s is heat capacity of the solid material, and T_0 is ambient temperature. The term $k_s \rho_s c_s$ is referred to as thermal inertia and is often determined as a single effective property based on ignition data [57]. Time to ignition is inversely proportional to the square of the external heat flux $\dot{q}_e{}''$. Using observed ignition to determine t_{onset} implies that the time required to mix pyrolysis products with surrounding gas, and to initiate the gas-phase chemical reaction, are

negligible. This justifies the formulation of the ignition problem into one related to the solid phase only.

Some limitations of this theory, especially regarding real-world combustion are: (1) the assumption of constant thermal inertia in the solid; (2) the need to define an ignition temperature; and (3) the incorporation of heat losses from the sample or fractional absorption of the heat flux [82,102]. Further, both models and experiments in fire science literature represent processes in a single dimension, assuming that the applied heat flux, the net absorbed heat flux, and mass transfer occur in the same direction.

4.2.3 Prior Models of Wood Combustion

Pyrolysis models used in previous studies have represented the relevant heat transfer, mass transfer, and pyrolysis reactions for ignition scenarios, finding that simulated mass release rates have the same general features as observed data [108–110]. Spearpoint and Quintiere derived an integral model to predict burning rate [87,111] and compared it with measured burning rates of four wood species with heat applied along and across the longitudinal grain. They fit values of ignition temperature, thermal conductivity, and heat capacity for each species and orientation. Inferred ignition temperatures were a factor of 1-1.5 times higher, thermal conductivities 2-6 times lower, and heat capacities 1-3 times higher when heat flux was applied along the longitudinal grain instead of across. All of these physical properties were fit using measured, time-dependent data; that is, they were "effective" properties rather than independent measurements.

Boonmee and Quintiere [112] reported measurements in which heat was applied along and across the longitudinal grain of a single softwood. Galgano *et al.* then used these measurements to

explore sensitivities in a model they developed [101]. They found that predicted ignition times had sensitivity to wood thermal conductivity and density.

Fawaz *et al* [52] compared the numerical model Gpyro [67] with mass loss for wood heated from four sides for several wood types. The portion of the model considered "quasi-steady-state" (Phase III in Fig. 1) matched measurements well, but the time dependence of mass loss prior to ignition – the subject of this investigation – was not as well modeled.

4.2.4 Goal of this Study

Many materials have been used to explore relationships affecting ignition of solid fuels. However, the material anisotropy is rarely explored due to sample preparation in standard methods. These simplifications may cause the findings to be unrepresentative for the case of real biomass in the context of cooking and heating appliances which are not an idealized one-dimensional problem. This work investigates the anisotropy of thermal and diffusive properties in wood by modifying the ratio of sample length to surface area of longitudinal grain exposed to a heat source for the purpose of achieving ignition.

4.3 Experimental Description

4.3.1 Experimental design

To assess whether theories of ignition might be useful to aid design of deliberate combustion devices during Phase I, we present pyrolysis and ignition experiments on a range of biomass samples, heat fluxes and sample orientations.

Scaling of time to ignition. To examine whether Equation (1) applies across wood types with different material properties, we conduct identical time to pyrolysis and time to ignition

experiments for biomass samples deliberately chosen for their range of properties (Section 2.2). Acceleration of pyrolysis or ignition was identified using mass loss rate (MLR), a common approach in the fire safety literature [113,114]. The rapid increased mass loss rates above the initial baseline observed during pyrolysis is herein referred to as pyrolytic acceleration. Ignition was confirmed visually (i.e., the initiation of a sustained flame at the surface of the fuel). This approach was favored over measuring surface temperature due to uncertainties in making T_s experimental measurements [115].

Ignition characterization. To assess how mass flux relates to characteristics of the pre-ignition period (Phase I, Fig. 1), we compared experiments with and without pilot flames, termed "ignition" and "pyrolysis" respectively. Prior work has compared behavior of pyrolyzing wood with and without a pilot flame for the purpose of determining spontaneous ignition [116]. However, studies comparing pyrolysis and ignition MLRs are limited and do not assess the orientation of longitudinal grain as a control variable for t_{py} and t_{ig}.

Heat and mass transfer resistance. We explore the possible influence of mass transfer on time to ignition by comparing three orientations for each type of biomass, designated in Figure 5. Terminology in this paper refers to the orientation of the longitudinal grain vector ($\hat{\boldsymbol{L}}$) when the heat flux was applied in the *z* direction. In samples labeled *LGx*, the grain parallelled the long dimension of the sample, exiting on the face with the smallest cross section. Most wood in the real world is burned in this configuration. In the *LGy* configuration grain was perpendicular to the heat flux and exited

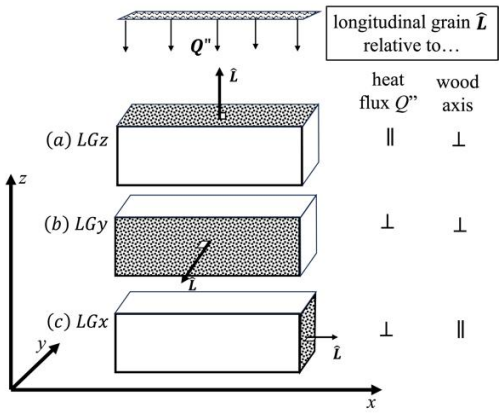

Figure 5. Wood grain orientation relative to incident heat.

the sample on the larger face. For the *LGz* configuration, grain was parallel to the heat flux and also exited on the larger face.

Wood is an anisotropic material in which thermal conductivity can be 1.5 to 2.8 times higher parallel to the longitudinal grain compared with conductivity orthogonal to the longitudinal grain [91,94]. Pyrolysis product is expected to escape the wood in the direction of greatest permeability, which occurs longitudinally, and this was confirmed by visual observation.

4.3.2 Biomass Sample Selection

Three hardwood types were selected to cover a large range of longitudinal permeabilities (Table 1). In order of highest to lowest longitudinal permeability, these woods were Red oak (*Quercus rubra*), Maple (*Acer saccharum*), and White oak (*Quercus alba*). In hardwood trees, long range mass transport of water occurs in tubular channels called vessels, and permeability in the direction of these vessels is high. One softwood, Scots pine (*Pinus sylvestris*, also known as European redwood) was compared with the hardwoods. Softwoods do not contain long tubular vessels, but are comprised of cells called tracheids, which are connected by small orifices through which longitudinal flow occurs. This structural difference results in lower average longitudinal permeability for softwoods than for most hardwoods [117].

Table 1. Wood density and longitudinal permeability with thermal inertia± and thermal conductivity (k) in the longitudinal and radial direction for the three hardwoods and one softwood.

Wood	Density (kg/m^3)	Longitudinal Permeability (Darcys)[a]	k_long (W/m-K)[b]	k_rad (W/m-K)	$k_s\rho_s C_s$ long (J^2/m^4-K^2-s)	$k_s\rho_s C_s$ rad (J^2/m^4-K^2-s)
Maple	705	7-10	0.33	0.16	269921	130871
Red oak	700	56-61	0.58	0.22	471042	178671
White oak	755	0.45-14	0.58	0.22	508053	192710
Scots pine	520	2.1	0.183	0.182	110405	109802

a. Hardwoods [117], softwood [118]

b. Oak: [119]; Maple:[94,120]; Scots pine: [121]

±. C_s = 1160 J/kg-K assuming T = 300 K for all woods. [94]

All samples were rectangular prisms with a cross-section (height times width) of 30 mm x 30 mm. Hardwood samples were 70 mm long and softwood samples were 90 mm long; the difference was due to the available wood stock material. The size of the samples is smaller than is typical for ignition and pyrolysis experiments. The sample dimensions were chosen to allow comparison of heat and mass transfer effects based on the direction of the heat flux and air flow relative to the wood grain, for which a large length-to-width ratio is required. Samples with knots and other blemishes were rejected to ensure these features did not affect the heat and mass transfer.

4.3.3 Heating Procedure

Experiments were conducted using the Fire Propagation Apparatus [122]. The FPA, shown in Figure 6, applies a known, constant heat flux to the surface of a solid in a stream of oxidizer of variable composition. The FPA was chosen because the ability to purge the sample chamber with a known flow rate of air ensured that each sample was exposed to a similar fluid flow environment. Prior to choosing the FPA exploratory non-piloted trials were conducted in a cone calorimeter, during which ignition was found to be piloted by the conical heater making investigation of

pyrolysis behavior unpredictable. The FPA therefore ensured pyrolysis tests would not auto ignite at the investigated heat fluxes.

The FPA sample chamber includes a sample basket in the center of four tungsten-halogen lamps. These lamps illuminate and heat the upper surface of the sample. A quartz tube 150 mm wide and 400 mm tall surrounded the samples to ensure an even flow regime around the wood. The tube was purged with a constant stream of air at 200 lpm, ensuring oxygen availability around the sample and preventing stagnation.

Samples were stabilized in the sample holder by placing the specimen in a round mesh basket with a diameter of 140 mm. Mass loss was measured by a load cell (Mettler-Toledo WM4002-L) underneath the sample chamber. Emission products were carried out of the quartz tube, and carbon monoxide and carbon dioxide concentrations in the exhaust were measured with gas analyzer (Servomex 4100, non-dispersive infrared). Data were recorded at 1 second intervals. Data presented here account for a delay of 32 seconds between emission from the sample and arrival at the CO and CO_2 analyzer.

Two heat fluxes— 30 kW m^{-2} and 40 kW m^{-2} – were chosen to represent normal cooking use. Users are unlikely to operate biomass stoves under conditions which result in long ignition delay times (i.e. low heat fluxes, $\leq$ 20 kW m^{-2}) and high external heat fluxes promote gas-phase autoignition ($\geq$ 50 kW m^{-2}) and are therefore not associated with release of unburned products. Tests were conducted both with and without a pilot flame. Autoignition never occurred at these heat fluxes, so samples in tests without a pilot flame represent pyrolysis only, and these tests are labeled “pyrolysis.” Throughout, piloted ignition was accomplished with a pilot flame at a ratio of 60:40 ethylene air mixture creating a blue conical flame 10 mm long at a position 15 mm above the center of the sample.

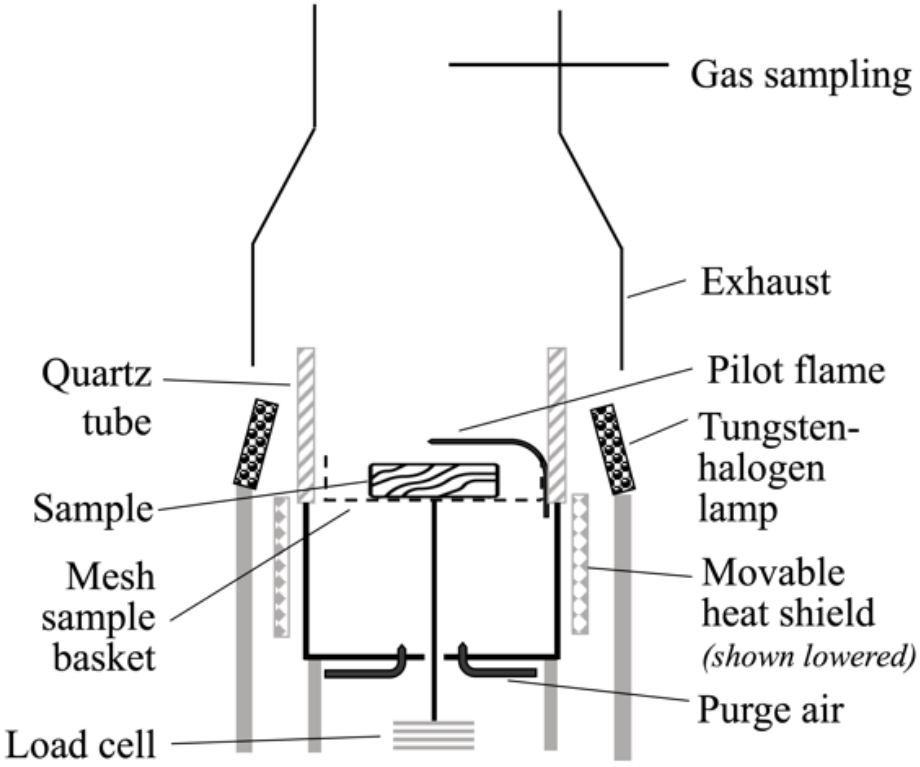

Figure 6. Schematic cross-section of the Fire Propagation Apparatus.

The test sequence involved installing the sample, raising a heat shield around the quartz tube, turning the lamps on to allow stabilization, and then dropping the heat shield. This shield removal marks a clear beginning for each test and is reported as time zero. The sample was observed visually during initial heating. For tests with pilot flames, the observed time of ignition was marked.

4.3.4 Analysis

Mass loss rates were derived from the time-resolved mass measurements. Mass data were normalized by the initial weight of the sample to account for differing densities and slightly different sizes. A simple differential of mass data traces was taken after smoothing with a 50-point

central difference moving average. Although smoothing filters can shift the time to ignition [123], the comparison of times between conditions is insensitive to such artifacts. Time to ignition was determined from tests with piloted ignition, and time to pyrolysis was determined from pyrolysis-only tests. Both times were determined by identifying when the mass loss rate began to increase above the average initial baseline. The time at which MLR began to increase was identified as t_{py} or t_{ig}, depending on the experiment type. Other methods were considered, including marking the ignition event from observation [122] and by using the second derivative [114]. The selection of our chosen method is discussed in the results section below.

Deliberate combustion of solid fuels requires external support, often in the form of kindling. Reduction of resources required for ignition such as kindling or lighter fluid can result in significant improvements to user experience [11]. We assess whether those differences are important in practical settings by determining energy requirements for ignition. Incident energy provided to the sample prior to ignition is calculated as the heat flux multiplied by the exposed area and by the time to ignition. We then compare the energy required for ignition with the energy released from combustion of the entire wood sample. An example calculation is provided in the APPENDIX.

4.3.5 Summary of Experimental Conditions

Table 2 shows the experimental conditions varied during this study. All combinations of variables (heat flux, wood type, end grain configuration, and experiment type) were measured. The experimental data set consists of 30 ignition and 23 pyrolysis trials at 30 kW m^{-2}, and 33 ignition and 25 pyrolysis trials at 40 kW m^{-2}, for a total of 111 experiments. A minimum of two trials were conducted for each condition, except for Scots pine in the *LGy* orientation at 30 kW m^{-2}.

Preliminary trials indicated data to be repeatable with an uncertainty of 15 – 30 seconds with 99% confidence (n = 7) compared to 19 seconds with 90 % confidence (n = 2). By reducing the number of trials per test condition, a higher number of experimental conditions could be evaluated with a limited number of samples.

Table 2. Test conditions used in these experiments.

Heat flux (kW m^{-2})	30, 40
Wood	Maple, Red oak, White oak, Scots pine
Longitudinal grain	*LGx*, *LGy*, *LGz*
Experiment type	Pyrolysis, piloted ignition

4.4 Results and Discussion

4.4.1. Observations

Figure 7 shows mass loss rate and exhaust CO and CO_2 concentrations for a single wood and heating condition (Maple *LGz* at 40 kW m^{-2}). The behavior during pyrolysis-only experiments displays general similarities to the case with ignition, showing a delay to the onset of pyrolysis, and a relatively constant mass loss rate, after an initial transient peak, with greater concentrations of CO than CO_2.

In all tests with an ignition pilot, gas-phase ignition ensued shortly after pyrolytic acceleration. Radiant heat flux from the flame then accelerated the pyrolysis reaction as seen in the mass loss rates, and CO concentrations decreased as it was oxidized to CO_2. The effect of char layer buildup in decelerating mass loss is more obvious in ignition tests than in pyrolysis-only

tests. The remainder of the discussion relies on mass loss rate alone, as CO and CO_2 evolved concomitantly.

No autoignition occurred at either 30 or 40 kW m^{-2} heat flux. Glowing or surface combustion throughout most of the event was not observed either; all combustion occurred in the gas phase until the very end of the event. At that point, solid-phase combustion commenced, and higher concentrations of CO were produced (as seen in Figure 7).

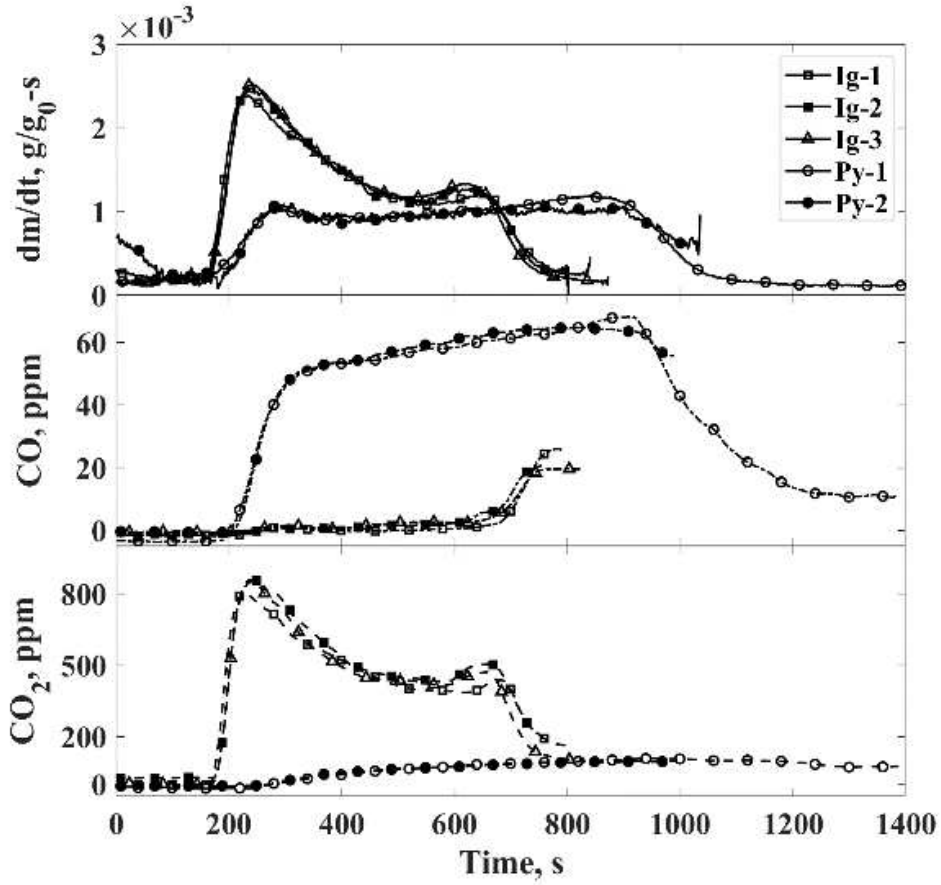

Figure 7. Mass loss rate, CO_2 and CO for Maple LGz at 40 kW m^{-2} with and without ignition. Square and triangle symbols represent different ignition trials. Circle symbols represent pyrolysis trials. Open and closed symbols represent trial 1 and 2. The third ignition trial is shown to emphasize repeatability of data.

Pyrolyzate was visually observed to leave the wood matrix on the face with the longitudinal wood grain exit, confirming that pyrolysis products traveled in the direction of greatest

permeability. Ignition occurred when pyrolyzate passed through the pilot flame; while heat transfer controlled the pyrolytic acceleration, macro-scale fluid dynamics also affected time to ignition. Pyrolyzate particles escaped prior to ignition for *LGx* and *LGy* directions, but not for *LGz*, because they were released more directly toward the flame. With a relatively small sample size, particles leaving the sample on any face were drawn into the pilot flame with little delay; this mixing is not certain in real-world combustion.

Times to pyrolysis and ignition were determined using mass loss rate profiles. Attempts were made to determine t_{py} and t_{ig} from the second derivative of mass loss data using methods reported in literature [114]. Large uncertainties were observed when determining the inflection point of the MLR curve using the second derivative. Finding t_{py} and t_{ig} from the time of increasing MLR acceleration relative to baseline was consistently possible with all data recorded and had lower uncertainties. The selection of this method came from the observation that ignition with flame feedback causes a sharp increase in the MLR similar to the increase in MLR observed during pyrolytic acceleration. Observation of an ignition event was not possible for pyrolysis tests, so previously reported methods were rejected to maintain consistency between the two experiment types.

4.4.2. Onset of Pyrolysis and Ignition

Pyrolysis-only and piloted-ignition tests were done under identical conditions to illustrate the separate influence of flame feedback. Figure 8 compares mass loss rates of pyrolysis-only and ignition experiments for three orientations and wood types selected to demonstrate a range of onset times.

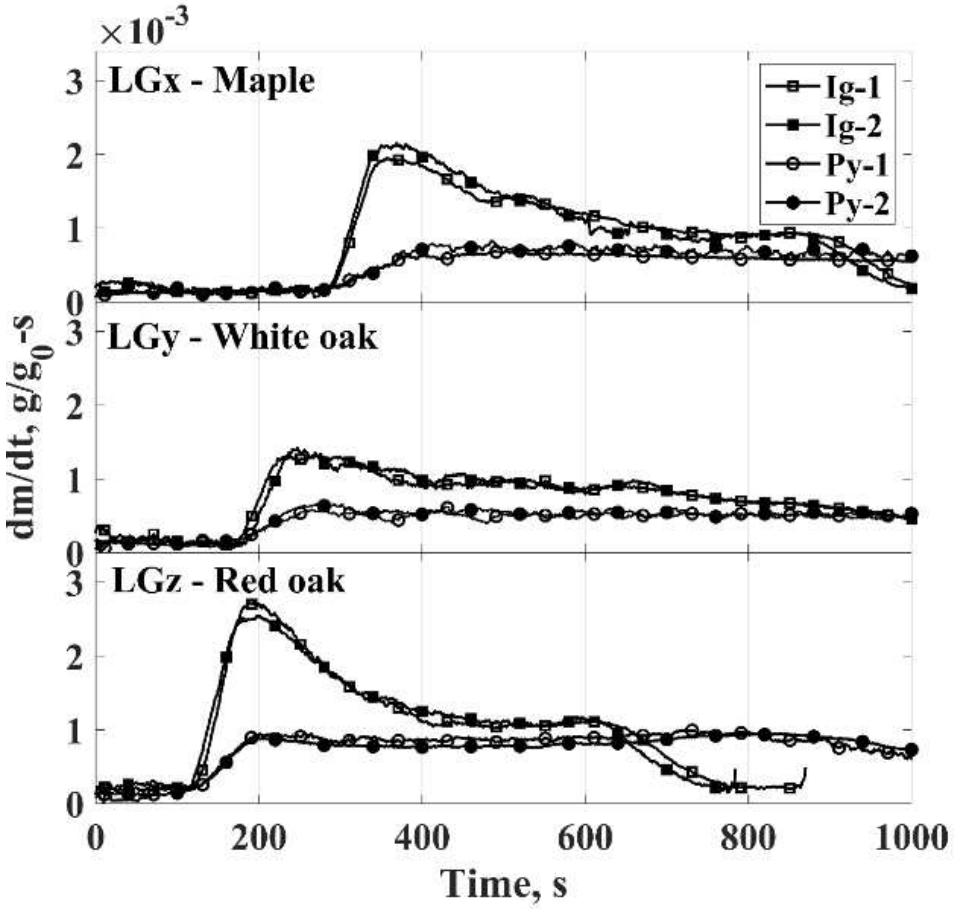

Figure 8. Mass loss rates during ignition and pyrolysis for three wood types and orientations at 30 kW m^{-2}. Conditions were selected to illustrate a range of onset times. Only the first 1000 seconds are shown.

For each condition, the time of MLR acceleration in the pyrolysis-only tests (t_{py}) occurs very near the same time as MLR acceleration due to ignition (t_{ig}) in the tests with a pilot flame. Although t_{ig} may sometimes appear slightly shorter than t_{py}, this comparison may be an artifact of the ability to detect the greater MLR associated with ignition. While Figure 8 shows only three illustrative cases, this coincident occurrence of t_{py} and t_{ig} is repeated in 24 paired pyrolysis and ignition tests.

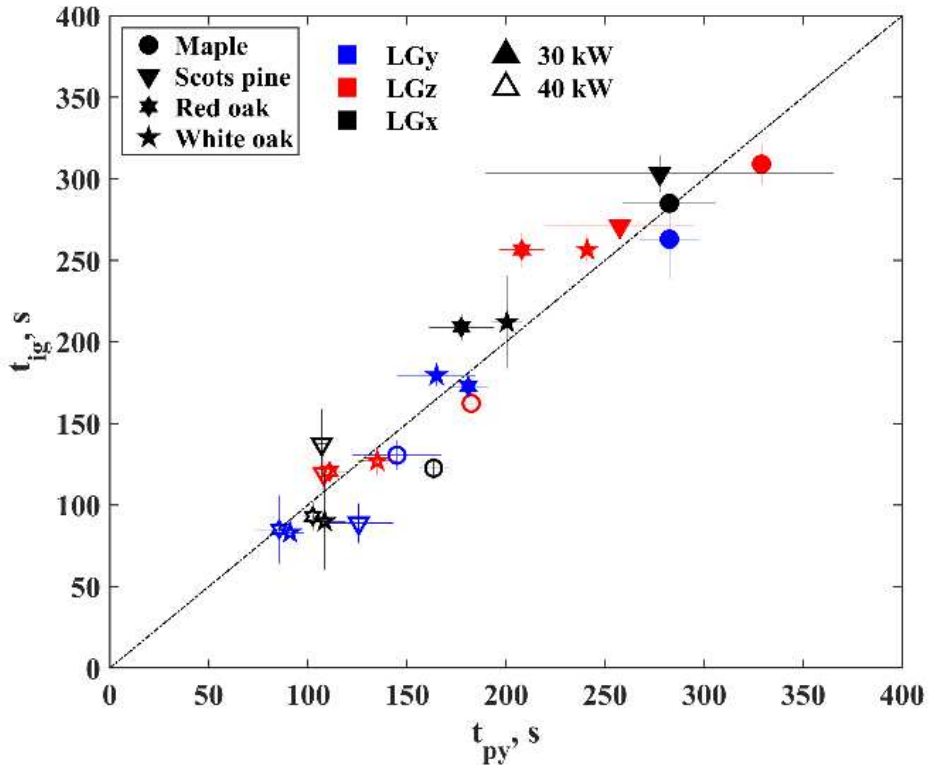

Figure 9. Parity plot comparison of tig and tpy for all tests. Symbols represent wood types, colors represent grain orientations, and filled versus open symbols indicate heat fluxes. Error bars indicate standard deviations for all trials at a single condition.

Figure 9 compares the two types of t_{onset} reported. T_{py} and t_{ig} are strongly associated across all conditions, with an R-squared value of 0.896. This comparison confirms the theoretical assumption underlying Equation (1): achieving pyrolytic acceleration is a limiting factor and can be detected even in experiments that never undergo ignition. Although gas-phase processes are certainly required to achieve flaming, the high correlation shows that time to pyrolysis dominates time to ignition under these conditions.

A common measure of ignition propensity is critical mass flux (CMF), or the mass flux observed at the time of ignition [64]. The principle behind this measure is that a minimum flux of combustible products is required to maintain gas-phase combustion, and therefore a specific mass flux of pyrolyzate, rather than a surface temperature, enables ignition. However, Figure 8 and

Figure 9 demonstrate that onset comes about before measurable mass flux occurs. If onset occurred after measurable mass flux, t_{ig} would lie consistently above the parity line in Figure 9. After ignition, flame radiation added to the imposed heat flux causes the MLR to increase faster than the pyrolysis-only condition. Much of the subsequent elevated MLR is a consequence of ignition rather than a cause. We conclude that the onset time, $t_{py,}$ is a better representation of limiting factors than is MLR measured near the time of ignition.

Figure 10 shows t_{ig} for all experiments as a function of thermal inertia ($k_s\rho_s C_s$) based on independent reports of these properties (Table 1). Time to ignition is presented because the reaction onset is more obvious in the time series; however, similar conclusions would follow from using t_{py}. Figure 10 also summarizes the level of repeatability; for each condition, times to onset were within 25 seconds for 44 of the 47 conditions, or within 14% of the 170-second average time to onset.

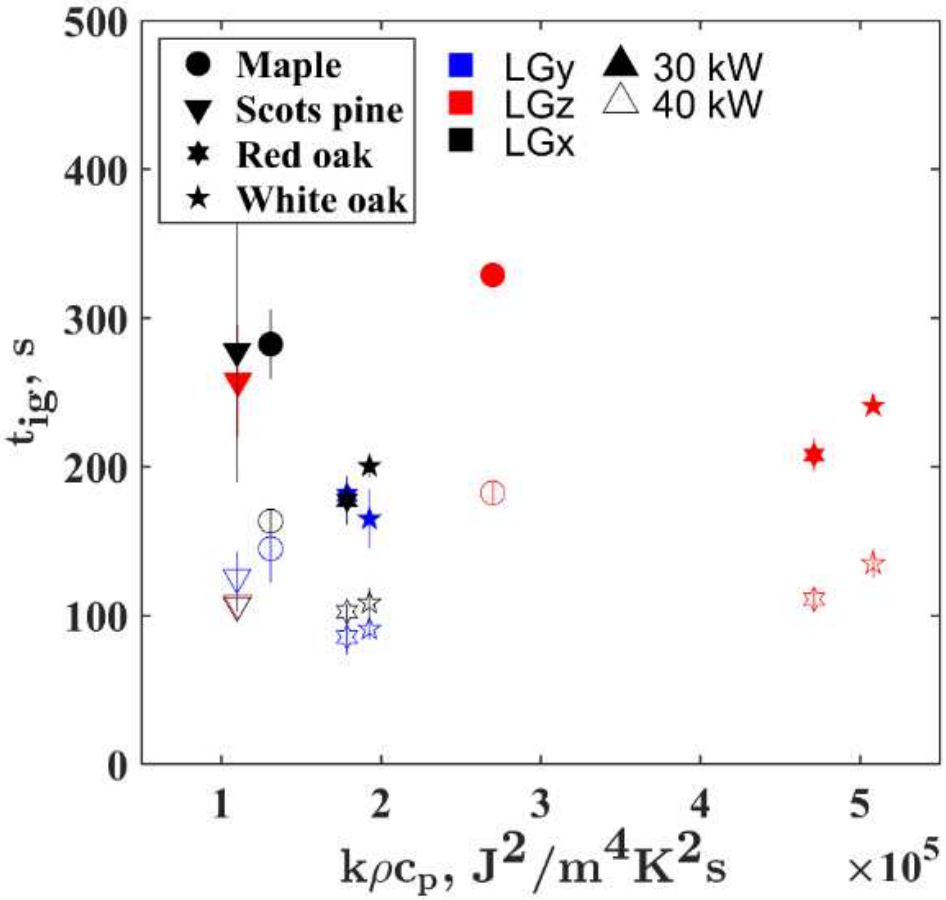

Figure 10. Time to ignition for all samples, including all grain orientations, woods, and heat fluxes. Symbols represent wood types, colors represent grain orientations, and filled versus open symbols indicate heat fluxes.

4.4.3 Minimal Influence of Permeability

For both *LGx* and *LGy* samples, external heat flux impinges perpendicular to the grain, so thermal conductivities should be identical. Like thermal conductivity, permeability is set by the wood microstructure [103] and is higher along the longitudinal grain. Transfer of pyrolysis products follows the path of least resistance, which is longest for *LGx* (see Figure 5). If permeability is a limiting factor in the overall reaction process, onset behavior of *LGx* and *LGy* samples (black versus blue in Figure 10) should differ. Instead, times to pyrolysis are similar between *LGx* and *LGy* for each wood. Although differences do appear, they are of the same order as the uncertainties. This observation suggests that permeability has little effect on the onset of

pyrolysis or ignition during Phase I. The deliberate choice of samples with a wide range of permeability increases confidence in this conclusion. This finding is unsurprising; resistance to mass transfer is most likely to influence behavior in later stages, when pyrolyzate is being driven out of the wood by elevated pressure, or when gas-phase mixing is required to achieve ignition [124].

Although differences between *LGy* and *LGx* are small and inconsistent, t_{ig} for *LGy* is often shorter. In both *LGx* and *LGy*, mass release occurs orthogonal to the incident heat flux. In the *LGy* configuration, the release area is greater than in *LGx*, which may increase the likelihood that pyrolysis products encounter the pilot flame. This influence of permeability and release area may play a greater role after the onset of ignition in less refined real-world combustion, which is not explored here. If a dependence on release area and gas-phase mixing exists, it would depart from the one-dimensional representation most often used to model ignition of materials.

4.4.4 Modest Influence of Thermal Inertia

The linear dependence of t_{ig} on thermal inertia expected from Equation (1) does not appear in Figure 10. Instead, a slight decrease of t_{ig} with increasing thermal inertia appears for similar conditions. For hardwoods, t_{ig} is consistently longer for *LGz*. This observation is consistent with the analytical prediction that increased thermal conductivity, which occurs in the longitudinal direction, leads to longer times to ignition [57,87,125]. However, the increase of 10-30% is much lower than expected based on reported anisotropic thermal conductivities, which differ by factors of 1.5 – 2.8. Vyas and Welker [125] found an approximate doubling in ignition time when heat was applied to the longitudinal grain direction as compared with the across-grain direction, but this magnitude of difference is not seen here. The softwood, Scots pine, has similar thermal inertia

in all directions, and its orientation does not influence onset time. In summary, the comparison of *LGz* with *LGx* and *LGy* onset times for the same wood supports a modest influence of thermal inertia on onset time, but that effect is not as strong as the linear relationship in Equation (1). Comparison across wood types does not support the theoretical relationship; if any dependence could be detected, it would be opposite to the prediction.

Prior evidence for scaling t_{onset} with material properties is limited, as Equation (1) is more often used to explain the influence of heat flux. Some studies have inferred effective material properties by combining experimental data with theoretical relationships like those underlying Equation (1), but those approaches cannot be used as independent confirmation of an expected dependence on material properties. Another reason for the predictive failure of Equation (1) is a difference of critical surface temperature T_s among biomass types, but if that is the case, then the relationship has limited utility in describing situations beyond specific experiments. Not only are tabulations of T_s lacking in the literature, but the measurement of surface temperature itself is subject to artifacts [102,115].

A final reason for failure of t_{onset} to scale with thermal inertia might be the assumption that all heat is transferred and not absorbed by the heat of reaction, or the inert-solid assumption [57]. This assumption has been shown to be incorrect; thermal decomposition is observed long before ignition [126], and Beaulieu and Dembsey showed that an inert solid behaved differently than a reacting solid [127]. Regardless of the reasons, the simple relationship expressed by Equation (1) implies that knowledge of biomass material properties may be useful in understanding ignition onset; we find this not to be the case.

4.4.5 Dominant Influence of Heat Flux

Time to ignition decreases, as expected, when comparing heat fluxes of 30 to 40 kW m^{-2}. Equation (1) might apply to changes in condition for the same material, even if it cannot be used to compare materials. Ratios of t_{py} were determined for each combination of wood type and orientation between the two heat fluxes. Across all wood types and orientations, $t_{py,30}/t_{py,40}$ ranged from 1.72 to 2.31 with a median of 1.86. These values are near the theoretical value of 1.78 determined from Equation (1). In the case of ignition, ratios of $t_{ig,30}/t_{ig,40}$ range from 1.90 to 2.80 with a median of 2.21. This higher value might be caused by the need to consider a critical heat flux offset in Equation (1) [109]. Another possibility is a differing influence of gas-phase mixing in the 30 kW m^{-2} case. The pyrolysis time ratio adheres marginally closer to theory than the ignition time ratio.

In summary, changes in external heat flux, but not measured wood properties, can be used to scale reported times to ignition for different woods. The lack of relationship with wood properties is less disadvantageous than it might seem. Because stove designers have no control over the wood types used, and users' choices depend on fuel availability, guidance for design independent of wood properties may be the most useful.

4.5 Implications for Deliberate Combustion

Are the differences in time to ignition reported here important in practical stove-use situations? We investigate this question using energy requirements for wood ignition (Section 4.3.4). As an example, *LGx* maple wood at 30 kW m^{-2} requires 404.3 kJ/kg to reach the onset of combustion (t_{ig}). Complete combustion of this wood sample would produce a heating value of 18227.5 kJ/kg. The energy ratio required for ignition is thus 0.0221 kJ/kJ of the energy ultimately

released. We refer to this value as the *ignition energy ratio* (IER); it represents a loss of efficiency in obtaining heat for the desired use (Equation (2)). A table of calculated ignition energy ratios and an example calculation is provided in the APPENDIX. Below we compare the ignition energy ratios of *LGz* orientations to *LGx*, since *LGx* represents the grain orientation in most conventional burning applications.

$$IER = \frac{energy\ required\ to\ achieve\ ignition}{energy\ produced\ by\ complete\ combustion\ of\ solid\ fuel} \quad (2)$$

4.5.1 Relative Importance of Time to Ignition Differences

The ignition energy ratio for maple wood *LGz* is 0.0240 kJ/kJ, which is 8.6 % greater than the ignition energy ratio for *LGx*. For red and white oak, the *LGz* ratio is approximately 20% greater than *LGx.* Scots pine has an 11% lower ignition energy ratio for *LGz* than *LGx* at 30 kW m^{-2}. Material type does affect time to ignition, but these differences may not be observable in practical situations. On the other hand, increasing the external heat flux from 30 kW m^{-2} to 40 kW m^{-2} produces a 40% decrease in the ignition energy ratio across all wood types. The more important reduction of ignition energy occurs when the incident heat flux is increased, rather than when material properties are altered.

The ignition energy may appear small compared with the heat released, but the ratios calculated in this way are minima, accounting for only incident heat absorbed by the sample. In realistic combustion geometries – as in experiments – a substantial amount of incident heat does not impinge on the sample and is lost to the surrounding environment. It is not hard to imagine a situation in which ignition requirements reach 10 % or more of the energy released by burning. This loss of efficiency is of similar magnitude to improvements sought by stove designers by other means.

The ignition energy ratios determined here depend on an assumed sample thickness (3 cm), or more broadly on surface-to-volume ratio. However, ignition energy ratios would retain the same relative values in different geometries or with different wood sizes, allowing comparison of different woods, orientations or heat fluxes across conditions.

4.6 Conclusions

This work presented experiments designed to isolate causes of variation in "real-world" wood and interpreted those experiments in the context of deliberate combustion. Comparisons of pyrolysis-only with ignition for identical wood types, configurations, and external heat flux show that achieving pyrolytic acceleration is a key factor preceding ignition. Experiments comparing three orientations of identical wood identify thermal conductivity, rather than permeability, as the main anisotropic property affecting time to pyrolysis and ignition. When wood grain is aligned with heat flux, thermal conductivity increases and time to pyrolysis is slower. Time to pyrolytic acceleration and ignition for different woods has an expected relationship with external heat flux but not with thermal inertia determined from wood properties.

The observation that pyrolytic acceleration is required prior to ignition may seem obvious but is generally assumed with very few demonstrations. Here, we have shown how those factors control pyrolytic acceleration and the sequential ignition of wood. Previous investigations of time to ignition for wood species used in practice have been able to produce plausible model-measurement comparisons by invoking effective material properties but not using independently-measured values. Comparisons may also have been dominated by the steady-burning phase at the expense of predicting pre-ignition behavior. These emphases may account for the apparent discrepancy between the perception that wood ignition is well understood and our findings that a

simple but extensive set of measurements does not conform to a well-accepted theory. This level of predictability can still be useful for designers of deliberate combustion devices. The use of fire science principles demonstrated for deliberate combustion in this work shows that some development is required to understand the relationship between pre-ignition pyrolysis and deliberate ignition.

Chapter 5

Particle measurements identify mechanisms in cold-start ignition of thermally-thick biomass

This Chapter contains material submitted to the Combustion Institute International Symposium on Combustion, 2026. If accepted, this work will be expanded in length and published in the Proceedings of the Combustion Institute. Co-authors include John J. Flynn, Rory M. Hadden, Tami C. Bond. My contributions were Conceptualization, Investigation, Data curation, Data analysis, Writing – original draft, review & editing.

5.1 Introduction

Smoke produced from wood burning contains particulate matter (PM) with diameters of 2.5 μm or less ($PM_{2.5}$). Household exposure to $PM_{2.5}$ released from biomass burning is ranked in the top three mortality categories, globally [2]. Premature death rates attributed to $PM_{2.5}$ exposure are especially high among women and children, who spend substantial time in cooking environments [128,129]. Efforts to reduce the amount of PM released in the cooking environment have included the design of improved cook stoves [17,42,130,131]. Ignition of large wood fuel creates an additional challenge for stove users in that tinder and kindling materials can be difficult to acquire [11].

While some studies have shown that cook stove improvements reduce emissions by up to 50% [18,20], Roden *et al.* identified that PM emission factors are two to three times higher in actual use than in simulated laboratory events [21]. They concluded that the ignition of wood in a cold stove may contribute to elevated emission rates.

Ignition of wood is described in fire science literature [54,56,57], where principles of heat and mass transfer are used to describe conditions for ignition. Additional works explore the

anisotropic transport phenomena associated with wood grain properties [87,97,125]. These studies have found that the lowest heat flux to support ignition of thermally-thick biomass is approximately 12 kW m^{-2} [60]. Ignition studies explore a wide range of heat fluxes, with 25 kW m^{-2} and below often considered "low" heat flux, typical experimental conditions ranging to 75 kW m^{-2}, and even higher fluxes used in some studies [58]. Fire-safety investigations focus on fire prevention and emphasize occurrence of ignition rather than PM emissions before and during ignition events. Thus, these works usually do not measure aerosol emissions or use them to diagnose ignition mechanisms.

Studies of PM emissions for atmospheric purposes tend to focus on total quantities emitted. Elsasser *et al.* partitioned wood burning into four phases corresponding to chemical signals measured with mass spectroscopy [50]. Haslett *et al.* reported emissions in piloted ignition studies [45], focusing on aerosol released at different stages of burning. Both studies showed that the transition from the endothermic chemistry of pyrolysis to the exothermic chemistry of a flame rapidly decreases the release of organic PM and increases refractory PM emissions (soot) [45,50]. However, at high heat fluxes these emissions simulate steady-state operation, not the mechanisms of PM release during cold start. Fawaz *et al.* used Gpyro software to predict organic aerosol emitted from pyrolysis [52]. Model predictions were accurate during the steady-state portion of burning but poorly predicted the transient ignition stage.

In summary, cold-start ignition can produce a large amount of organic PM, increasing human exposures. The goal of this work is to identify burning mechanisms that can reduce those exposures. By "mechanisms" we mean reproducible, empirically-distinguishable phenomena in which heat, mass, and reaction principles govern inception and cessation. The word "burning" recognizes that the determining factors may occur in the solid matrix (pyrolysis), the gas phase, or

interactions between the two. Recognizing mechanisms, for example, could lead to reducing organic PM by altering pyrolysis, by forcing condensed tars to pass through a flame, or by promoting ignition at low heat flux.

Prior work [97,107] has shown that samples exposed to relatively high heat fluxes (30 and 40 kW m^{-2}) undergo a rapid increase in mass loss, which we term "pyrolytic acceleration," after a period of delay. Pyrolytic acceleration occurs regardless of whether gas-phase ignition follows, and is a necessary condition to achieve ignition. The present paper contributes to the overall goal by exploring burning mechanisms at lower heat fluxes that simulate cold-start ignition, using fire-science experiments that also leverage observations of particulate-matter emissions.

5.2 Experimental Methods

The experiments described here combine a design common in fire science with measurements of aerosol emissions. The experimental design draws on our prior work that leveraged sample orientation and anisotropic properties of fuel to isolate the influence of material properties [97]. The final data set consists of 24 samples across two heat fluxes, two grain orientations, and two woods.

5.2.1 Wood sample preparation

Samples were cut into two grain orientations. Wood prepared with the longitudinal grain (*LG*) running the length of the sample are referred to as *LGx*, as seen in Figure 11. This grain orientation is the conventional way wood is burned in a cook stove. Samples were also prepared with the longitudinal grain along the height of the sample (*LGz*). This sample preparation

maximized the amount of longitudinal grain facing the heat source and altered the thermal conductivity in the direction of heat flux.

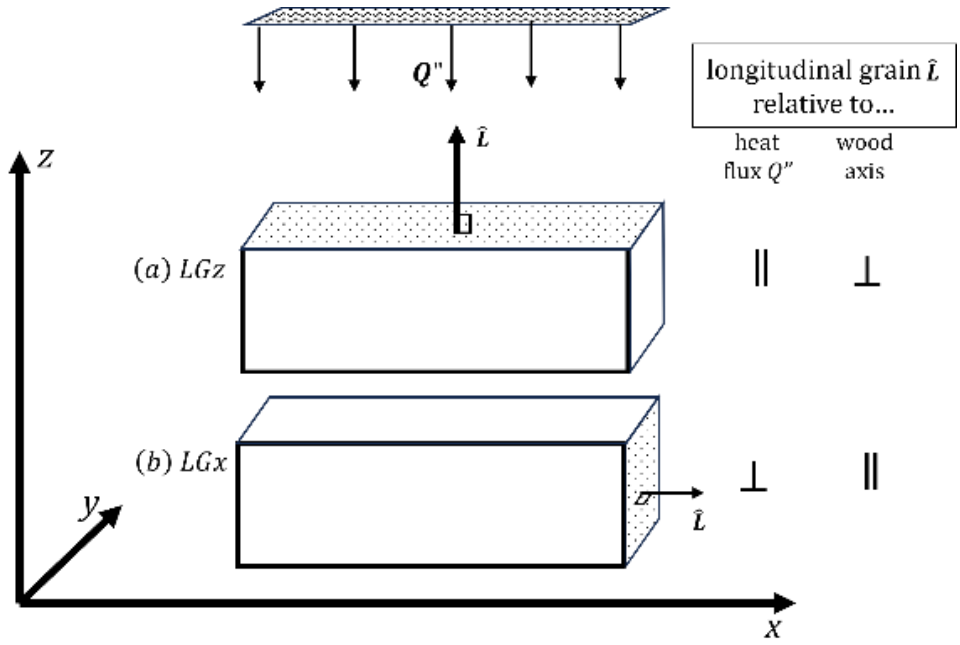

Figure 11. Schematic showing wood grain orientation relative to incident heat flux.

White oak (*Quercus alba*), a hardwood, allowed investigation of the influence of anisotropic heat and mass transfer, as thermal conductivity and permeability are different in along-grain and cross-grain directions for hardwoods. Douglas fir (*Pseudotsuga menziesii*), a common fuel, provided a comparison with the very different structure of softwoods. Samples were considered "dry" with a moisture content ≤ 6 %. Comparing the two sample orientations can be used to investigate behavior of samples with differing thermal properties.

5.2.2 Heating apparatus

The Fire Propagation Apparatus (FPA) was used, and the operational procedure has been previously described [122]. This experimental apparatus was chosen in part because it can separate pyrolysis behavior from ignition. Experiments were contained within a quartz tube providing an air environment at a flowrate of 200 lpm. Heat fluxes of 15 kW m^{-2} and 20 kW m^{-2} were chosen to mimic the low heating conditions typical for cold-start ignition.

A load cell (Mettler-Toledo WM4002-L) was used to measure the mass of a burning sample. Each specimen was placed in a mesh sample basket measuring 140 mm in diameter. A heat shield was raised shrouding the sample. The lamps were turned on to preheat the surrounding area while gas and aerosol sampling equipment was staged for data collection. The beginning of the test, t = 0 s, was marked by the dropping of the heat shield. Mass loss rate (MLR) was determined by taking the derivative of the mass curve.

Experiments were conducted with and without a pilot flame, which was positioned 15 mm above the center of a sample. Tests without a pilot flame ("pyrolysis") demonstrated sample behavior in response to external heat flux alone. Tests with a pilot flame ("ignition") determined whether the release of pyrolysis gases was sufficient to support a flame and introduced flame feedback to the sample.

5.2.3 Gas and aerosol sampling

A CO and CO_2 analyzer (Servomex 4100) measured concentrations of each gas. Aerosol was sampled with a diluting probe from the plume located at the outlet of the quartz tube. Particle size distributions were measured in the diluted gas using an Engine Emissions Particle Sizer (TSI EEPS 3090). Number counts in each size bin were integrated to obtain total number concentration,

as well as particle mass concentration assuming spherical particles and a particle density of 1.4 g cm^{-3}. Dilution ratios ranged from 12.8 to 27, depending on experimental conditions. Aerosol concentrations shown here are adjusted to the test-specific dilution ratio. Gas concentrations were sampled at 0.55 Hz and particles were sampled at 1 Hz. Data were adjusted for differential travel time in the sampling tubes.

Figure 12 shows laboratory air and pilot flame backgrounds of particle mass and particle number as measured by the EEPS. The pilot flame is shown to produce particles during operation. Initial operation of the pilot flame results in the production of a large number of particles of small mass. A steady decline is observed until a steady-state release is observed around 700 s. This is likely caused by the start-up of the FPA system and pilot flame probe in a cold laboratory space. To compensate for the cold surroundings the FPA was preheated prior to daily testing.

Around 1150 s the pilot flame was turned off allowing for background collection of ambient particles. Particle mass and particle number for test conditions without a pilot flame show a significantly lower release compared to measurements with a pilot flame. This example reinforces the use of pyrolysis-only data to observe particle release prior to the ignition event. Tests utilizing the pilot flame were pre-heated so that the probe and surrounding FPA components were stable before testing. Background PM and PN for both experiment types are then considered negligible since the signal produced by wood emissions are multiple orders of magnitude higher than these background levels.

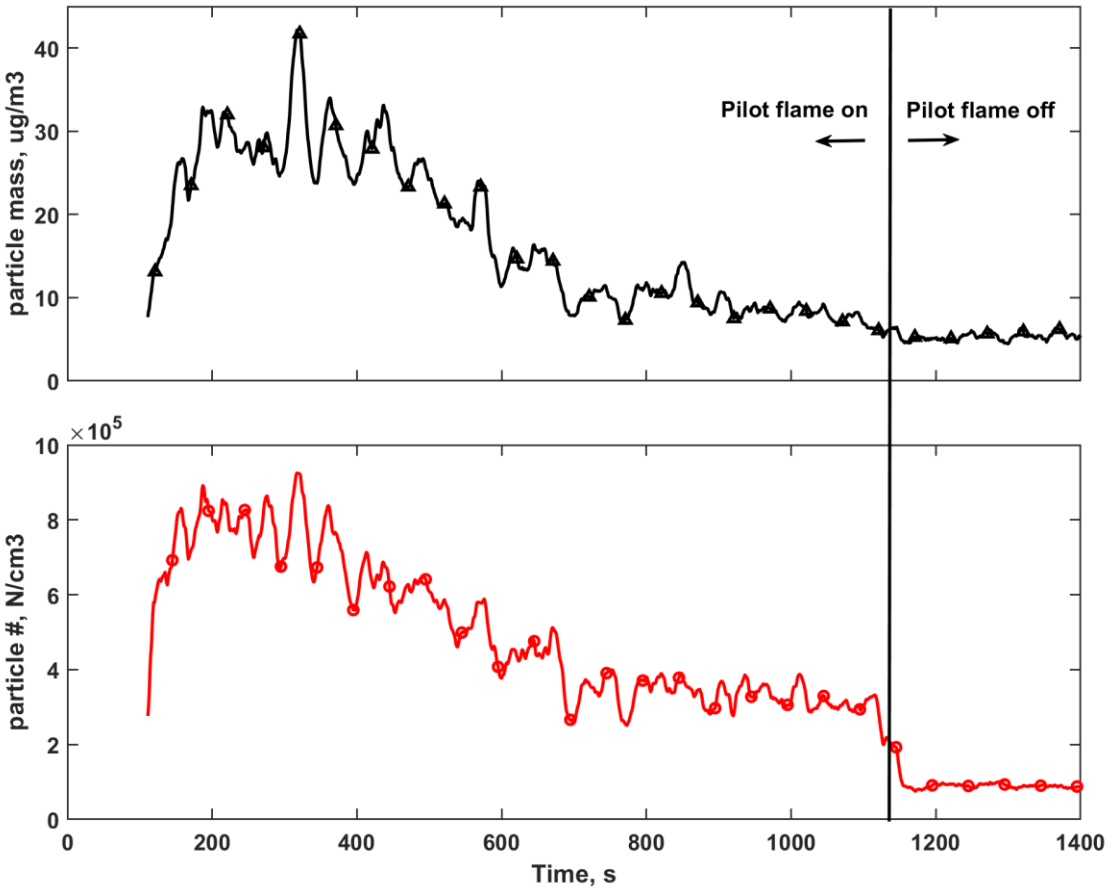

Figure 12. Particle mass (top, black) and particle number (bottom, red) for EEPS background collection at 15 kW m^{-2} with and without a pilot flame. Vertical line indicates the time at which the pilot flame was turned off.

5.3. Results and Discussion

5.3.1 Relationship between pyrolysis and ignition

Pyrolysis and piloted ignition of white oak at 20 kW m^{-2} are shown in Figure 13 for the *LGz* grain orientation. MLR begins at a baseline and exhibits a distinct acceleration at around 850 s. When a pilot flame is present, this accelerated mass loss enables gas-phase ignition, which produces CO_2. Radiation feedback from the flame then accelerates pyrolysis, as seen by the rapid increase in MLR and CO. Without a pilot flame, no CO_2 is produced and mass loss and CO production continue at a slow rate.

In all tests reported here, as well as in prior work [97], the same conditions that yielded pyrolytic acceleration also produced ignition when a pilot flame was present. Conversely, the pilot flame failed to produce ignition under conditions where no pyrolytic acceleration occurred without a flame.

Prior to gas-phase ignition, pyrolyzate or condensable tar forms particles that can escape the burning zone. After ignition, these particles may react in the gas phase to form CO_2. While flames do produce soot, a component of $PM_{2.5}$, emission factors of soot are usually much lower than those of organic matter. In the following sections, we present results from pyrolysis-only tests to examine the behavior of particle emissions prior to pyrolytic acceleration.

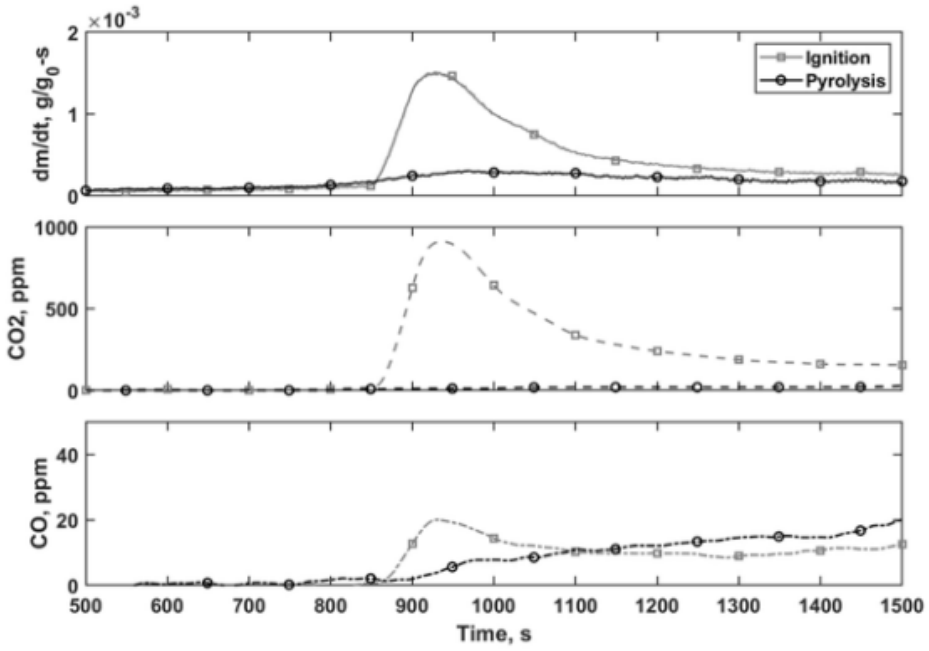

Figure 13. Mass loss rate of white oak under pyrolysis (Py, circles) and piloted ignition (Ig, squares) at 20 kW m-2.

5.3.2 Pre-ignition behavior at low heat fluxes

Figure 14 shows mass loss rate (MLR), particle mass, and particle number released during pyrolysis of white oak in *LGx* and *LGz* orientations at 15 kW m^{-2}. CO_2 does not rise above

background. MLR appears constant for the first 1700 s for both orientations, and pyrolytic acceleration appears for the *LGz* around 1700 s. Pyrolytic acceleration never appears in the *LGx* configuration, although slightly elevated mass loss appears after about 3600 s. Release of CO begins about the same time as the mass loss.

Particle number (PN) tells a different story. Around 1000 s particle number begins to increase for both *LGx* and *LGz*. This increase in particle number, with only a small elevation in particle mass concentration, is caused by the release of very small particles with diameters of about 60 nm. Their appearance indicates that the fuel surface temperature has increased enough to begin breakdown or volatilization, but the resulting particle concentration is not high enough to achieve rapid coagulation and particle growth. These particles are observed even before a change in MLR is distinguishable.

The increase of particle number continues until about 1000 s. At this time, a maximum PN followed by a decline is observed for *LGz*, while particle mass continues to increase as particles grow into the 160-nm diameter range. This opposing change in PN and PM is likely caused by a decrease in nucleation and condensation of pyrolyzate onto existing nuclei.

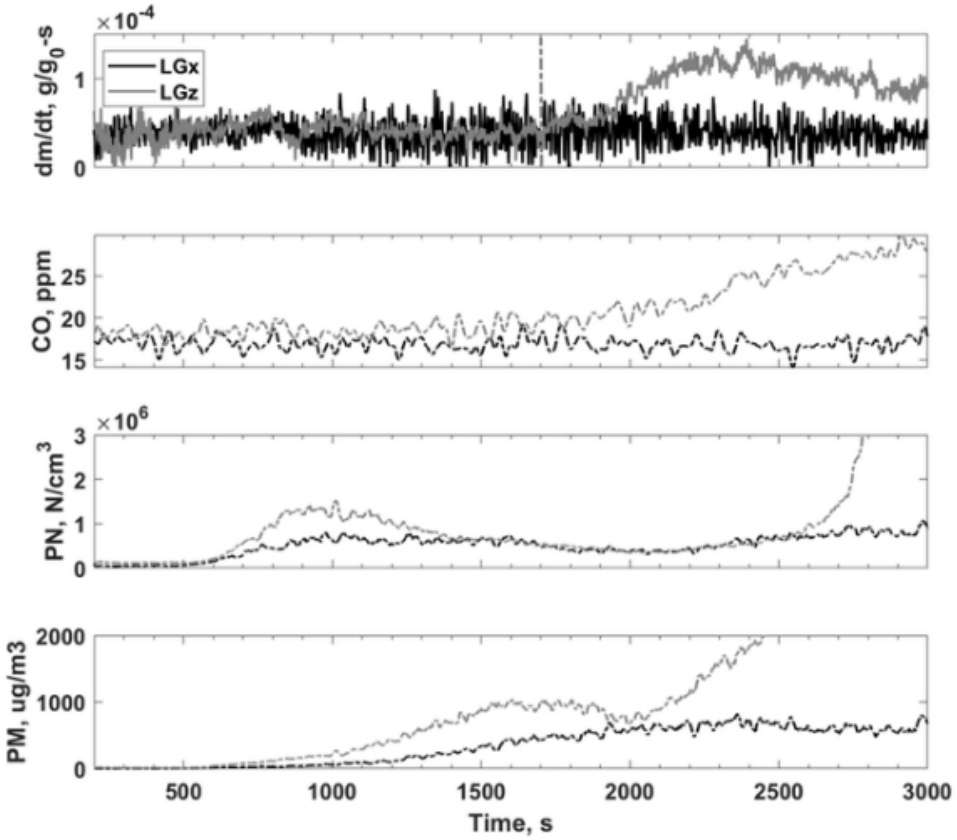

Figure 14. Mass loss rate (top panel), particle mass (second panel), particle number (third panel), and CO concentration (fourth panel) of LGx (black) and LGz (grey) for white oak pyrolysis at 15 kW m^{-2}. A dashed vertical line on MLR indicates tpy.

At the time of pyrolytic acceleration in *LGz*, 1700 s, total particle mass concentration drops before rising again, while PN stays relatively constant. This event appears to mark a shift to a reaction that produces both particles and CO, different from the early reaction that produces particles alone.

Later in the burning process of *LGz,* around 2500 s, particle concentration rises as the flame dies down and gas-phase reactions decrease (smoldering). While this mechanism is also of interest for human exposure, the present work focuses on combustion behavior before and after pyrolytic acceleration.

We now focus on the comparison with *LGx*, which never undergoes pyrolytic acceleration despite having the same heat flux and wood type as *LGz*; the only difference between the two is

the orientation of the material, and thus the material properties in the direction of heat flux. While particle number and then particle mass occur at the same times in these tests, concentrations are only about half as high. Whether the reduced magnitude in *LGx* is caused by differences in specific surface areas or in resistance to sub-surface mass transfer cannot be determined from these data. The reaction that produces CO at the expense of PM, causing a dip in the PM mass concentration, never begins in the *LGz* experiment.

Results from pyrolysis of douglas fir at the same heat flux (not shown) reproduce several aspects observed in Figure 14. PN emissions begin first, followed by an increase in PM. For *LGz*, an increase in CO production occurs along with a momentary dip in PM, a prelude to pyrolytic acceleration. For *LGx*, PN and PM emissions occur at the same time as for *LGz*, but at a lower rate. Neither the CO-producing reaction nor pyrolytic acceleration occur in *LGx.* The two woods differ in the shape of the PM "bump" prior to CO production but are similar in all other respects.

5.3.3 Particle size during early release

Figure 15 shows the particle size distributions for incremental time steps during pyrolysis in the *LGx* and *LGz* grain orientations. At 0 s and 500 s particle size distributions indicate very little release is occurring. By 1000 s a distinct change has occurred which shows high numbers of particle counts centered around 60 nm. This is consistent with nucleation mode particle sizes. Coupling release at 1000 s to mass data (Figure 14) shows the particle release at this stage is consistent with the maximum particle number observed prior to pyrolytic acceleration. By 1500 s the number of particles released have decreased and the particle size distribution has broadened and is centered above 100 nm. Figure 14 shows a decrease in particle number as particle mass increases. The growth of particle size to 100 nm and the broad distribution of particle diameters at

this time step indicates condensation of volatile fuel release onto nucleation particles has begun, marking a shift to accumulation mode particles.

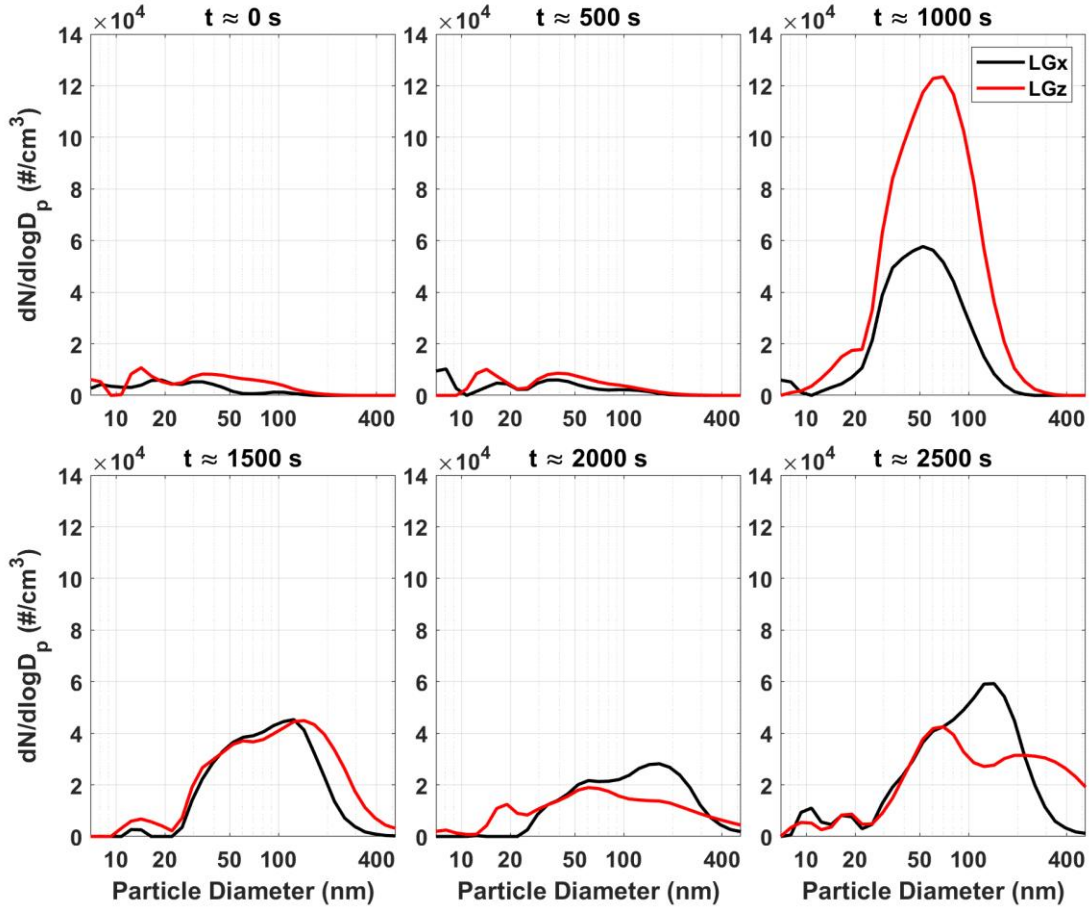

Figure 15. Particle size distributions for white oak pyrolysis at 15 kW m^{-2} at incremental time steps.

Profiles at t = 2000 s shows minimal release is occurring at this stage. This is confirmed in Figure 14 which shows the release of PN and PM decreases while pyrolytic acceleration occurs. These data indicate that while a rapid increase in mass loss occurs little change to particle nature is observed. Simultaneously, CO concentrations begin to increase from a baseline release. This shows that the nature of fuel released during the onset of pyrolytic acceleration is consistent with the production of high volatility gases which do not contribute to particle growth.

By 2500 s a notable shift has occurred between the two grain orientations. Particles released from the *LGx* sample stay centered above 100 nm with a slight shoulder observable at 60 nm. This distribution shows that nucleation mode particles are present but a significant shift to accumulation mode diameters has occurred. Particles released from *LGz* samples have a strong bimodal signal, with particle counts observed in two distinct size ranges centered on 60 nm and 200 nm. This is explained by the presence of the pyrolytic acceleration event. Rapid release of mass allows for two simultaneous processes to be observed: (1) formation of nucleation mode particles caused by a large flux of volatile and semi-volatile organic compounds which aid in gas-to-particle condensation, and (2) the release of low volatile organic compounds which drives rapid particle growth via condensation and coagulation mechanisms, resulting in accumulation mode particles.

5.3.4 Effect of increased heat flux

Figure 16 shows the mass loss rate, particle mass and particle number released during pyrolysis of *LGz* white oak at 20 kW m^{-2}. Tests done at 15 kW m^{-2}, one of which appeared in Figure 14, are included for comparison. The figure also serves to illustrate reproducibility; although the time series of MLR are not exactly the same after pyrolytic acceleration, the features and timing are similar.

Pyrolysis at 20 kW m^{-2} demonstrate the same sequence of events that appeared in Figure 14, but accelerated. Release of PN occurs first, followed by an increase in PM as particles grow. The reaction that produces CO follows, and is associated with pyrolytic acceleration around 750 s. The apparently slight increase of 5 kW m^{-2} has a strong impact on pyrolysis mechanisms at low heat fluxes. At 20 kW m^{-2}, pyrolytic acceleration occurs sooner, and fewer particles are released

over a shorter time. In addition, the inhibition of pyrolytic acceleration for *LGx* orientation, which appeared at lower heat fluxes, does not appear at 20 kW m^{-2}.

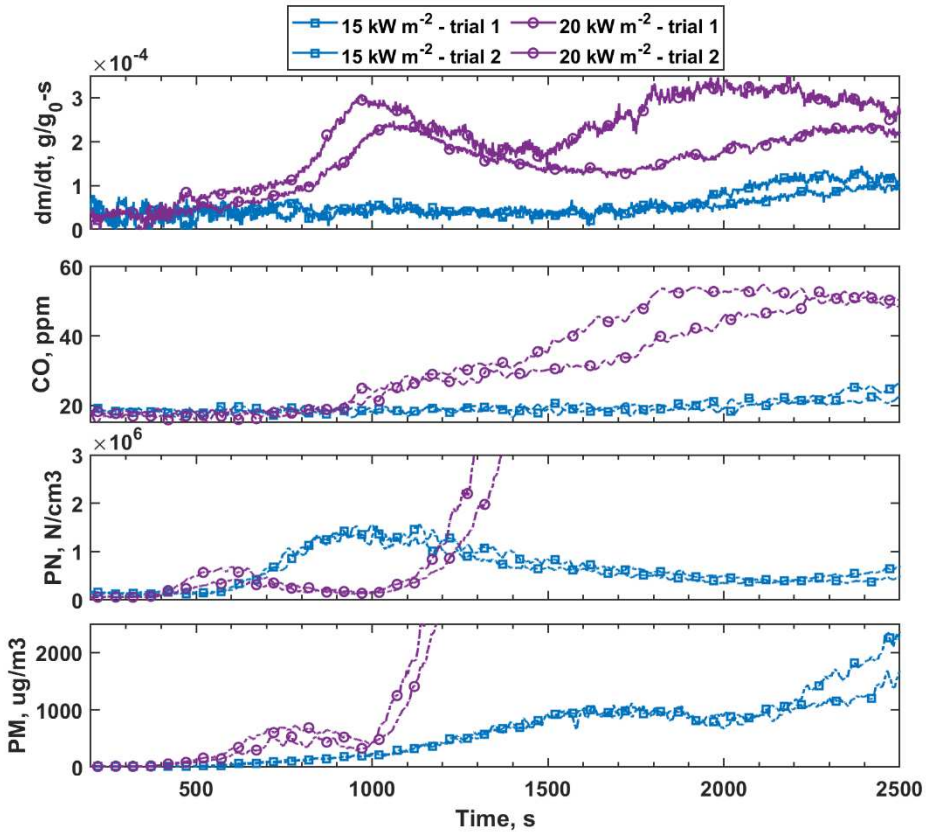

Figure 16. Mass loss rate (top panel), CO concentration (second panel), particle number (third panel), and particle mass (fourth panel) in white oak pyrolysis in *LGz* orientation at 15 kW m^{-2} (blue) and 20 kW m^{-2} (purple).

One possibility for the early mechanism of particle emission is a simple release of matrix-bound volatile matter, similar to water evaporation. The comparison of 15 kW m^{-2} and 20 kW m^{-2} tests shows that this is not the explanation; if it were, a similar integrated particle mass would be emitted prior to pyrolytic acceleration.

Figure 17 shows the particle size distributions for incremental time steps observed during pyrolysis at 20 kW m^{-2} in the *LGx* and *LGz* grain orientations. On first glance, profiles for all *LGx*

and *LGz* grain orientations time steps exhibit similar particle release distributions. At t = 0 s little activity is observable. Advancing to t = 500 s shows a strong signal centered on 60 nm for both *LGx* and *LGz*. The particle size distribution at t = 1000 s is unremarkable, with evidence that particle release has temporarily reduced which is consistent with the PM and PN profiles shown in Figure 16. MLR at t = 1000 s is at a maximum for *LGz*, which suggests that products released at the initial maximum MLR at 20 kW m^{-2} are high volatility gases. In the sequence of t = 1500 s, 2000 s, and 2500 s, the particle size distributions show similar behavior between the two wood grain orientations. A bimodal signal is produced which indicates the presence of both nucleation and accumulation mode particles. The similarity between the particle size distributions for each wood type suggests that the dominant burning mechanism at 20 kW m^{-2} is different than the mechanisms involved at 15 kW m^{-2}.

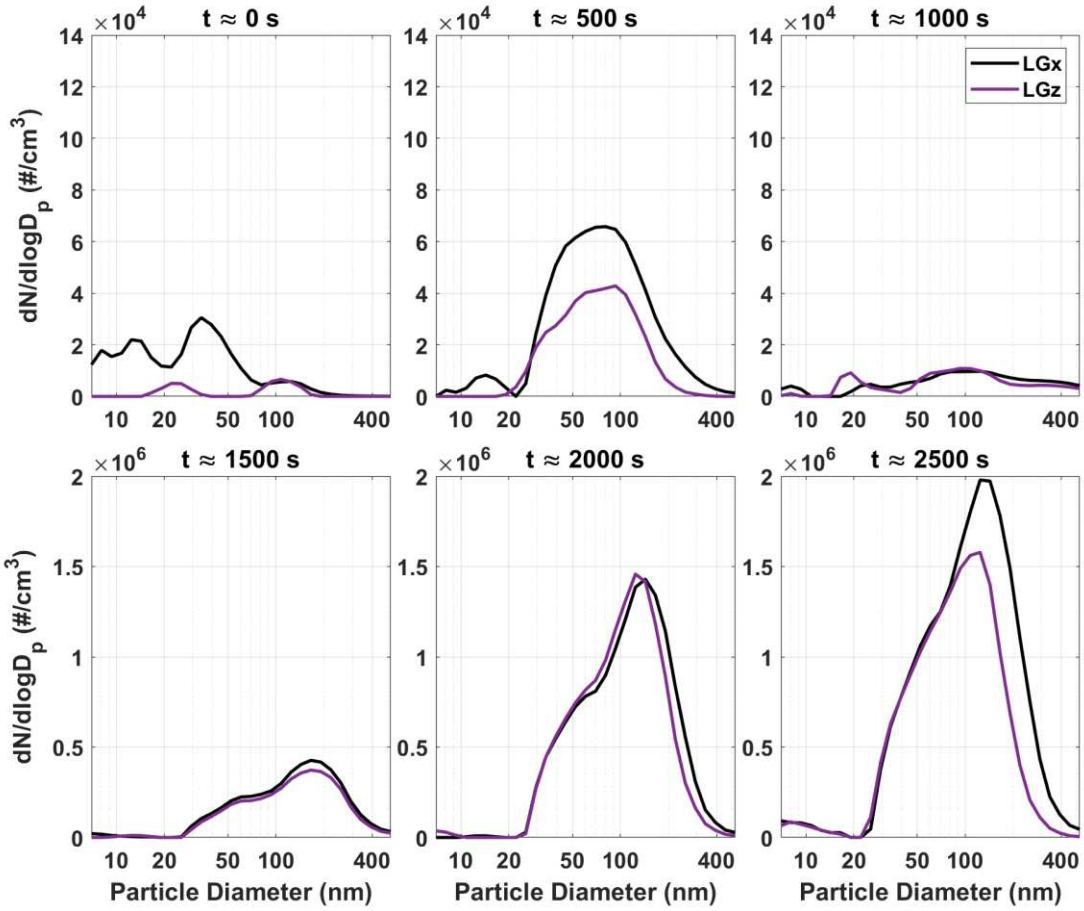

Figure 17. Particle size distributions for white oak pyrolysis of *LGx* and *LGz* at 20 kW m^{-2} at incremental time steps.

5.4 Summary

This work reports an expanded characterization of fire-science experiments to identify how particulate matter is released prior to ignition of thermally-thick solid fuel. We identify a mechanism that releases first small particles, then greater particle mass, before giving way to another reaction that generates both CO and condensable material. This mechanism could not have been identified with standard measurements of mass loss rate alone. The early mechanism is lengthened at low heat fluxes (15 kW m^{-2}), allowing emission of more particles prior to establishment of a gas-phase flame, and may operate even when ignition is impossible.

Recognizing the need for minimum heat flux and the influence of orientation may support practical guidance for reducing the exposure of stove users.

Chapter 6

Toward a principle-centered understanding of smoke exposure reduction from deliberate combustion of wood

This Chapter contains material prepared for submission to Fire Safety Journal. Co-authors include John J. Flynn, Rory M. Hadden, Tami C. Bond. My contributions were Conceptualization, Investigation, Data curation, Data analysis, Writing – original draft, review & editing.

6.1 Introduction

A 2016 study estimates that 2.67 billion people globally heavily rely on solid fuels in the indoor home environment for cooking [132,133]. Compared to 1990 reports of household air pollution exposure, improvements have been made to reduce exposure to particulate matter in the size range of 2.5 μm ($PM_{2.5}$) by approximately 10 %. Updated values approximate 111 million disability-adjusted life-years (DALYs) in 2021 due to household air pollution, alone [133]. Effectiveness of intervention efforts is summarized by Quansah, et al. as an improvement for personal exposure levels, which are still far above World Health Organization guidelines [15]. While improved stoves and implementation programs have made a lot of progress possible, investigations of deliberate combustion methodologies is an underutilized approach at improving exposure levels.

The ejection of $PM_{2.5}$ into the surrounding environment generally falls into the domain of the atmospheric science community. An active subset of atmospheric studies report findings on $PM_{2.5}$ emissions including sources of exposure [33,40], measurement methods [8,100], emission types [134], and observed benefits from improved technologies [14,134,135]. This characterization of $PM_{2.5}$ release aids in policy development [14] and implementation methods [16]. Assessment of

burning mechanisms connected to the creation and prevention of $PM_{2.5}$ is under-reported. Especially detailed studies will associate flaming and smoldering with emission types, but neglect to attribute fire principles to the release of mass which forms PM.

In contrast, studies of fire safety identify phases of burning that have characteristic rates of reaction, heat release, and product release. Specific mechanisms of heat and mass transfer, as well as evolution of the solid matrix, demarcate these phases. The goals of fire safety studies are typically avoiding ignition or understanding flame spread, and to the best of our knowledge, scientific understanding of each phase has not been leveraged to reduce particulate emissions and user exposure.

The goal of this paper is to identify conditions that lead to a high risk of human exposure, and to identify remedies for those conditions. We first review the phases as understood in fire-safety literature and describe how their governing mechanisms might affect exposure (Section 2.1). Next, we briefly summarize prior analysis [31,53,97,136] that constrains phase-specific emission behavior (Section 2.2).

Solving the massive problem of human smoke exposure from deliberate solid-fuel combustion will require improvement in diverse mechanisms and specific situations. The body of work summarized here is a contribution to this endeavor, although it does not complete it.

6.2 Background

6.2.1 Description of burning phases

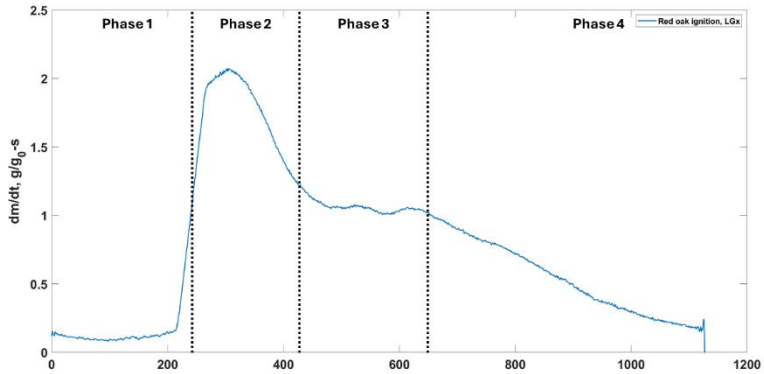

Figure 18. Phases of solid combustion identified in fire science literature and their relevance to deliberate combustion and smoke release. Labels tpy and tig on the x-axis refer to the conventional onset of pyrolysis and of ignition, respectively.

Burning phases have been identified for solid-fuel combustion, as shown in Figure 1 [45]. These burning phases are clearly visible in the time profile of mass loss rate (MLR). In this section, we outline these phases as they appear in the near-infinite solids used in fire-safety studies, and compare the behavior with that expected in deliberate combustion.

Phase I, initiation: The first phase begins with the onset of heat exposure (t = 0 s). During this phase, the wood is warmed to a temperature that supports rapid reaction. In prior work, we showed that the onset of rapid reaction, which we term "pyrolytic acceleration," is a necessary precedent to ignition [97]; under identical conditions, pyrolytic acceleration occurs at approximately the same time whether or not gas-phase ignition occurs. Pyrolytic acceleration marks the end of Phase I. In fire safety literature, the duration of Phase I is known as "time to ignition."

Phase II, acceleration: Mass loss rate continues to accelerate as long as the heat flux is applied. The MLR may be sufficient to sustain a gas-phase flame if the products are ignited, and these exothermic reactions add heat flux to the solid matrix, further increasing MLR. As the reaction front proceeds into the solid matrix, a char layer that is more insulating than the virgin wood builds

up, slowing heat transfer and the progress of the reaction. This phase ends when heat transfer through the char layer becomes the limiting factor for reaction. Due to its greatly varying MLR, this phase is known as “transient” in fire safety science.

Phase III, stabilization: Once heat transfer through the char layer becomes the limiting factor, the MLR remains relatively stable; it slowly decreases due to the gradual thickening of the char layer. A gas-phase flame is maintained with sufficient MLR. This phase is known as “steady state” in fire safety science, and provides ideal operation for a user who relies on heat flux for a particular application such as cooking. In finite solid matrices, such as those in deliberate combustion, MLR may increase again instead of remaining steady if thermal waves from opposing sides intersect. The reaction rate may also respond to the formation of cracks in the char layer. Phase III terminates with extinction, discussed below.

Phase IV, extinction: Extinction begins either when virgin biomass is no longer available to become pyrolysis product, or when virgin fuel remains but its release rate is no longer sufficient to sustain a flame. Under low heat flux, extinction may even occur immediately after Phase II if the MLR cannot support a flame.

2.2 Relevance of burning phases to particulate matter release

Products of pyrolysis include permanent gases such as carbon monoxide (CO) and condensable tars; when tars condense or nucleate in the cooler ambient air, they form organic particulate matter. About 20-30% of mass lost from the solid matrix becomes condensable organic matter at temperatures 500 ºC and below [53]. Chemical composition of the released particles

varies little throughout Phase II and III, although it does depend on wood type and environment temperature [31].

Each phase governs the production of particulate matter from a pyrolyzing, burning wood matrix differently. When gas-phase reactions (flames) are present, they greatly reduce the amount of organic particulate matter, but may also increase the quantity of soot or black carbon. In this section, we again discuss the first three burning phases, this time with attention to influences on PM release.

Phase I, initiation. Prior to pyrolytic acceleration, mass loss and particle release directly from the biomass is modest. However, we previously identified burning mechanisms that release PM before pyrolytic acceleration [136] and before gas-phase reactions are present to consume them. These releases, first with high number concentration and then with increasing mass, appear unavoidable because they are part of a sequence leading to pyrolytic acceleration.

An important source of PM and other emissions in a cold-start situation is kindling or fire-starter, needed to produce heat that raises the biomass temperature. Fire-starting materials are considered difficult to source and the burden of identifying solutions to scant materials often falls to women and children [11]. Over-harvesting of kindling and tinder requires stove-users travel far distances to find resources. Avoiding PM release during Phase I thus involves minimizing the energy required for ignition. In prior work, we showed that time-to-ignition did not have a predictable relationship with fuel thermal conductivity, but it did decrease as imposed heat flux increased.

Phase II, acceleration. The acceleration or transient phase is characterized by a peak in MLR, with a rapid increase and drop. The MLR peak is not an outcome of ignition, as it appears even in the absence of gas-phase combustion. When a flame does occur, it increases heat flux and MLR

peak height, produces soot (black carbon) through fuel-rich combustion, and oxidizes pyrolysis products. However, the rapid changes in pyrolyzate ejection rate make successful gas-phase mixing and thermal oxidation difficult to maintain, and both soot and pyrolysis products can escape the reaction zone. It may not be possible to eliminate PM release during this period, but minimizing it can be accomplished by limiting variation in MLR, and ensuring that ignition can occur as soon as pyrolytic acceleration occurs.

Phase III, stabilization. After a layer of char is formed, the pyrolysis front proceeds into the depth of the wood, releasing mass at a nearly constant rate. This steady release can support a stable flame, removing particulate matter release can occur on the surface. Minimizing PM2.5 exposure during this phase III entails delaying extinction as long as possible and ensuring that products pass through a flame. If extinction occurs while virgin wood is still available in the matrix, released product can form organic PM, similar to PM formed in Phase I. Additional creation of PM can come from the extinction of local flamelets while the remaining wood continues to burn. This causes the escape of PM-containing smoke to be released at a location spatially removed from existing flames.

6.3 Experimental Methods

This work draws on two sets of experiments that have been previously analyzed for other purposes. Each series was completed during a visit of several weeks at a collaborating laboratory (University of Edinburgh), with a fixed amount of time available on the testing apparatus. In the first set, the experimental design explored time-to-ignition and isolated the separate influences of permeability and thermal conductivity, across four wood types, by manipulating sample orientation as described in Section 3.2 [97]. Analysis of this data set showed a limited influence

of material properties and of permeability, and differences between softwood and hardwood behavior [97].

The second data set was designed to explore release of particulate matter, especially at lower heat fluxes. Fewer wood types and only two orientations were compared in this data set, and measurements of particle mass and number were added [136].

6.3.1 Grain Orientation

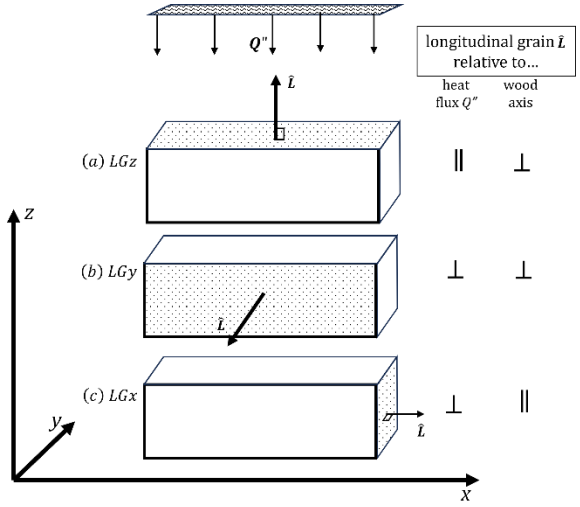

Figure 19. Schematic showing wood grain orientation relative to the incident heat flux on the sample.

An external heat flux was applied to each sample in a single plane, as described in the next section ("Heating Procedure"). The orientation of the wood grain relative to the plane of the heat flux was used to isolate the influence of permeability and thermal conductivity. Figure 19 details three types of wood-grain orientation relative to the plane of heat flux. The wood grain is represented by the longitudinal grain vector ($\hat{\boldsymbol{L}}$). These two orientations are described by the axis on which the longitudinal grain (LG) is oriented. As shown in Figure 19, the grain of the *LGx* samples, ran parallel to the long dimension of the sample, exiting on the face with the smallest cross section. Most real-world wood is burned in this configuration. In contrast, the grain for the

LGz configuration exited the sample on its larger face. If the pyrolysis product escaped in the direction of the greatest permeability, it would travel along the longest dimension in *LGx* samples and along the shortest dimension in *LGz* samples. If spatial mass transfer is a limiting factor in ignition by a pilot flame, the behavior of *LGx* samples would be expected to differ with the *LGz* orientation.

6.3.2 Sample Selection

Table 3 summarizes the tests across different wood types, orientations, heat fluxes, and use of a pilot flame. Hardwoods were white oak (*Quercus alba*), red oak (Quercus rubra), and maple (Acer saccharum). Softwoods were Douglas fir (*Pseudotsuga menziesii*) and Scots pine (Pinus sylvestris, also known as European redwood). Details of material properties and comparative behavior are given in prior work [97,136]. The structure of hardwoods results in greater anisotropy than in softwoods, and only that breakdown is summarized in Table 1.

Table 3. Summary of tests done at each condition. I and P denote number of tests with a pilot flame leading to ignition (I) and without a pilot flame (P). Asterisk (*) on the first line indicates that pilot flame always led to ignition and auto-ignition never occurred without a pilot flame. S and H denote number of softwood versus hardwood tests.

	Heat flux (kW/m^2)			
Orientation	**15**	**20**	**30**	**40**
LGx	4I, 4P	4I, 4P *	13I, 9P *	14I, 9P *
	4S, 4H	4S, 4H	10S, 12H	11S, 12H
LGy	-	-	9I, 6P *	9I, 8P *
	-	-	2S, 13H	5S, 12H
LGz	5I, 4P *	5I, 5P *	8I, 11P *	8I, 9P *
	5S, 4H	5S, 5H	7S, 12H	4S, 13H

White oak (*Quercus alba*) and Douglas fir (*Pseudotsuga menziesii*) were chosen to compare the behavior of a hardwood with a softwood. These woods have wide interest in

applications beyond deliberate combustion and serve to represent the structural properties inherent to hardwoods and softwoods. This structural difference results in lower longitudinal permeability for softwoods than for most hardwoods [118].

All samples were rectangular prisms with a cross-section (height times width) of 30 mm x 30 mm. Sample lengths were 70 mm. Samples with knots and other blemishes were rejected to ensure even absorption of heat and release of pyrolytic material.

6.3.3 Heating Procedure

The FPA has been previously described in the literature [122]. The sample chamber was purged with a constant stream of air at 200 lpm, ensuring oxygen availability around the sample and preventing stagnation. The use of air as a pyrolysis atmosphere was selected to remain consistent with conventional fire science experimentation and that of a real-world user. The test sequence involved installing the sample, raising a heat shield around the quartz tube, turning on the lamps to allow stabilization, and then dropping the heat shield. This shield removal is reported as time zero. Samples were mounted in the FPA using a mesh basket. Mass loss was measured by a load cell (Mettler-Toledo WM4002-L) underneath the sample chamber.

Mass loss rates (MLR) were derived from the time-resolved mass measurements. Mass data were normalized by the initial weight of the sample to account for differing densities. A simple differential was taken of mass data traces after smoothing with a 50-point central moving average. Although smoothing filters have been shown to shift the time to ignition [102,123], the comparison of features on MLR profiles between each condition is insensitive to such artifacts.

The experiments cover four heat fluxes: 15 kW m^{-2} and 20 kW m^{-2} from the second data set, chosen to represent cold start-up conditions; and 30 kW m^{-2} and 40 kW m^{-2} from the first data set, chosen to represent firebox behavior at realistic operating conditions but higher temperatures.

A unique feature of both data sets was pairing experiments done with identical conditions with and without a pilot flame, as summarized in Table 3. Autoignition never occurred at these heat fluxes, so samples without a pilot flame degraded by pyrolysis only. This design allowed separation of the influence of flame feedback.

6.3.4 Emission sampling

Emission products were carried out of the quartz sample tube, and carbon monoxide and carbon dioxide concentrations in the exhaust were measured with gas analyzers (Servomex 4100, non-dispersive infrared). Data was recorded at 1 second intervals. Data presented here account for a delay of 16 seconds between emission and the CO and CO_2 analyzers. Particle size distributions were measured by diluting the emission plume using a dilution probe, before sampling with an Engine Emissions Particle Sizer (TSI EEPS 3090). Number counts in each size bin were integrated to obtain total number concentration. Particle mass concentration was determined assuming spherical particles and a particle density of 1.4 g cm^{-3}. Dilution ratios were dependent on experimental conditions and ranged from 12.8 to 27. Aerosol concentrations are adjusted to the test-specific dilution ratio.

The final combined data set consists of 146 tests and approximately 147 hours of real-time measurements of mass loss, CO and CO_2. 34 tests and 55 hours also include real-time mass and number.

6.3.5 Ignition energy ratio analysis

The ignition energy ratio (IER) of a specimen is defined as the ratio of energy required to achieve ignition to the energy produced by the complete combustion of solid fuel, as shown in equation 1. Sample calculations are shown in supplemental information for a previous work [97].

$$IER = \frac{energy\ required\ to\ achieve\ ignition}{energy\ produced\ by\ complete\ combustion\ of\ solid\ fuel} \qquad (1)$$

Sample weights are determined from species density and sample dimensions. The energy required for ignition is determined for a specified heat flux and time to ignition (t_{ig}) in kJ. Energy produced by complete combustion of solid fuel is determined using the Lower Heating Value (LHV) for each fuel type.

6.3.6 Summary of Experimental Conditions

Experimental conditions varied during this study include 15 and 20 kW m^{-2} heat flux, *LGx* and *LGz* grain orientations, and pyrolysis and piloted ignition tests. All combinations of variables (heat flux, wood type, end grain configuration, and experiment type) were measured. Experimental data collected from the FPA consists of 17 pyrolysis and ignition trials at 15 kW m^{-2}, and 17 pyrolysis and ignition trials at 20 kW m^{-2} for a total of 34 tests. A minimum of two trials were conducted for each condition with repeats conducted when needed.

6.4 Results and Discussion

6.4.1 Mass transfer limitations in Phase I

Figure 20a shows mass loss rates of white oak at 15 kW m^{-2} in the *LGx* and *LGz* grain orientations in pyrolysis and piloted ignition experiment types. MLRs follow a baseline release for

the first 1500 s. Around 1500 s *LGz* samples show a pyrolytic acceleration and, when piloted, a subsequent ignition event that induces flame feedback. For *LGx*, MLR never rises above the baseline rate, regardless of whether a pilot flame is present. Particle measurements and surface discoloration confirm that reactions occur and mass is released in both configurations [136], although particle release is slower in the *LGx* orientation.

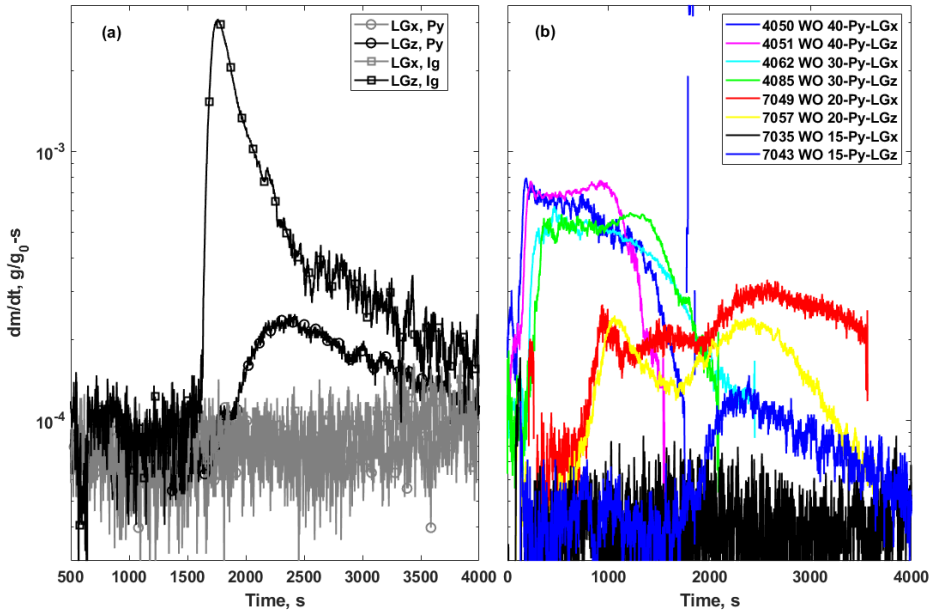

Figure 20. (a) White oak pyrolysis (circle symbols) and piloted (square symbols) mass loss rate at 15 kW m^{-2} in *LGx* (grey) and *LGz* (black) grain orientations. (b) White oak pyrolysis of *LGx* and *LGz* in heat fluxes of 15, 20, 30, and 40 kW m^{-2}. Data are plotted on a logarithmic axis for easier viewing.

In *LGz* samples, heat is applied parallel to the grain, thermal conductivity is higher, and pyrolysis products escape through a shorter path, compared with *LGx*. More than one hypothetical mechanism could be invoked to explain pyrolytic acceleration in *LGz* alone, such as faster penetration of heat into the solid, priming the matrix for reaction; or retention of product within the solid matrix in *LGx*, providing different reaction pathways. However, these hypotheses cannot be rigorously confirmed with these observations. Charring, discoloration, and increased

absorptivity of the wood surface is another change during this period [Chaos, 2014; Bal, 2013], but this occurs for both sample types.

At 20 kW m^{-2} and higher heat fluxes, *LGx* and *LGz* both undergo pyrolytic acceleration (Figure 20b). Although the dichotomous behavior at 15 kW m^{-2} is not definitively explained, we observe that this heat flux is a "borderline" condition for ignition. That is, physical properties of the wood either allow or prevent pyrolytic acceleration, but its occurrence is not guaranteed. During the time before ignition, PM is emitted from the wood itself as well as from kindling materials. The user experience of waiting 1500 s (nearly half an hour) is less than satisfactory. While ignition may eventually occur, and has elsewhere been reported to occur as low as 12 kW m^{-2} [60], these borderline conditions should be avoided to minimize PM exposure. However, it is informative to know ignition will eventually occur for *LGz* in low heat flux heating scenarios.

6.4.2 Ignition energy ratio across heat fluxes

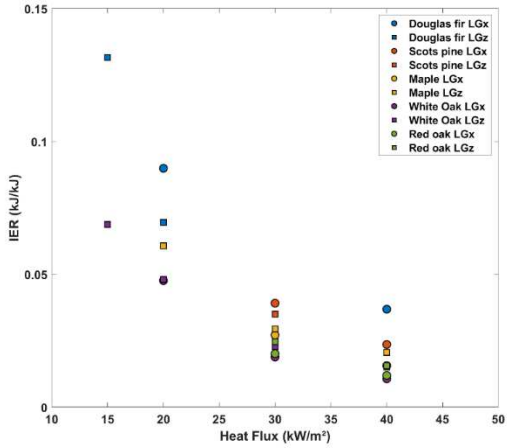

Figure 21. Ignition energy ratios (IER) for five wood types in the *LGx* and *LGz* wood grain orientation.

Figure 21 shows the ignition energy ratio (IER) for five wood types in the *LGx* and *LGz* grain orientations. At 15 kW m^{-2} and 20 kW m^{-2}, IERs range from approximately 0.05 to 0.14. IERs at 30 kW m^{-2} and 40 kW m^{-2} are below 0.05. IER for *LGx*, which did not ignite, is not included.

Figure 22 shows a box and whisker plot of IERs for softwoods and hardwoods at 15, 20, 30, and 40 kW m^{-2}. IERs for softwood are higher at all heat fluxes compared to hardwood IERSs. Lower heat fluxes of 15 and 20 kW m^{-2} show higher average IERs compared to 30 and 40 kW m^{-2}. For each wood type at any single heat flux no overlap of the interquartile range is shown, indicating a significant difference between hardwood and softwood. Additionally, comparison of each wood type for all heat fluxes shows no overlapping of the interquartile ranges. Heat flux is shown here to cause a significant change to IER for all wood types and grain configurations, combined.

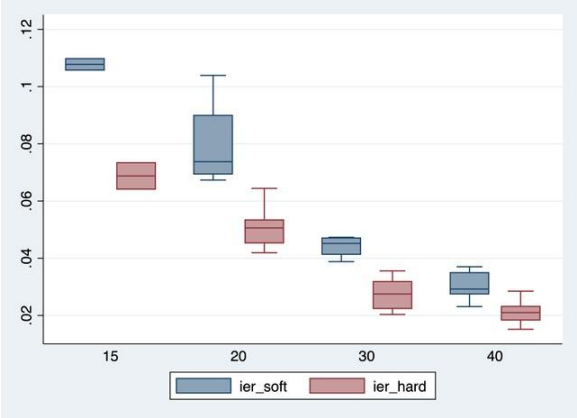

Figure 22. Box-and-whisker plot of IERs for softwood (blue) and hardwood (red) at 15, 20, 30, and 40 kW m^{-2}.

Heat fluxes below 30 kW m^{-2} are associated with high IERs, while heat fluxes 30 kW m^{-2} and higher produce low IER for these test conditions. Comparatively higher IERs for softwood at each heat flux is explained by the higher average thermal conductivity for hardwoods compared to

softwoods, independent of grain orientation. While in a practical setting these differences may not be noticeable, this is informative for utilizing thermophysical properties of wood for deliberate combustion. Practically, the boundary of 30 kW m^{-2} is a "sweet spot," producing enough heat to achieve ignition but not requiring faster consumption of tinder and kindling materials, which may be difficult to source for the end-user.

6.4.3 Achieving constant heat production

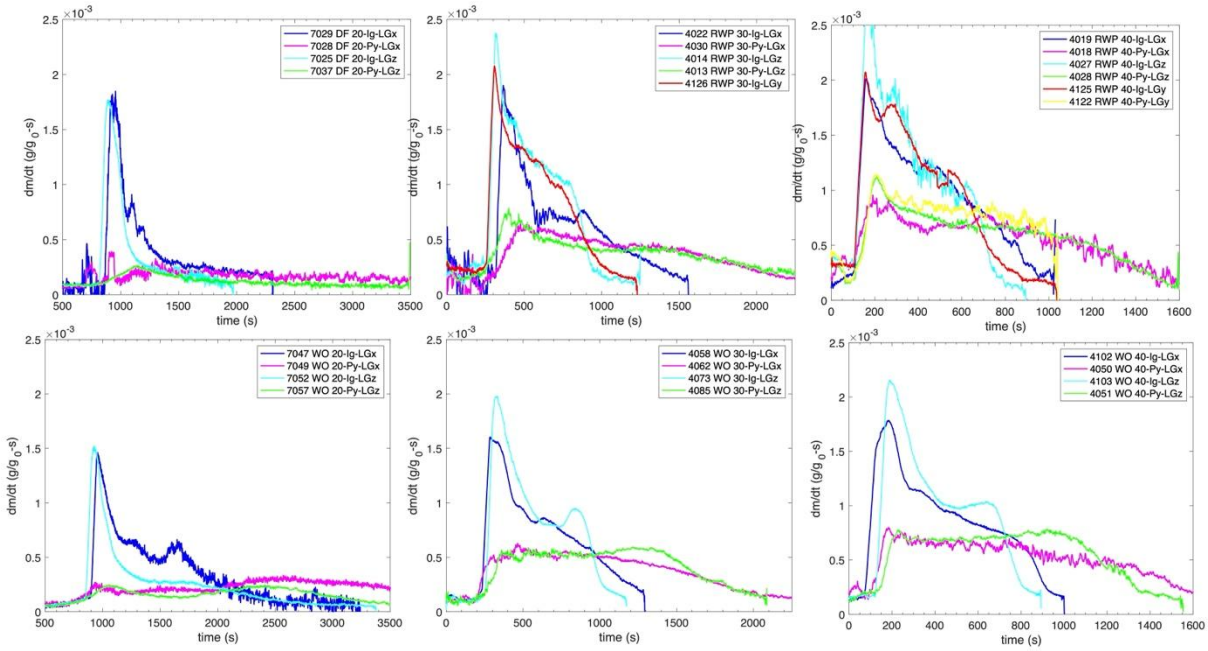

Figure 23. Mass loss rates for softwood (top row) and hardwood (bottom row) at fluxes of 20, 30 and 40 kW m^{-2} (left to right). Each figure shows piloted ignition and pyrolysis for all orientations measured.

Figure 23 compares MLR time series from ignition and pyrolysis at a range of heat fluxes. Although the transient peak (Phase II) draws the eye more readily, here we emphasize the ability to operate in Phase III, the portion after the peak ends and before extinction occurs. During an ideal Phase III, MLR would remain relatively consistent, providing prolonged energy for tasks that

require constant heat, like cooking. Constant MLR would also produce a stable flame more conducive to low particulate matter emission.

In piloted ignition tests, the portion of the curve after the transient peak is not always easy to distinguish, but when it is apparent a comparison between piloted-ignition and pyrolysis-only curves indicates the influence of flame feedback. Presence of a flame increases mass loss rate by up to 100%, and none of the increases are as great as the difference between pyrolysis-only MLR at 20 and at 40 kW m^{-2}.

Pyrolysis-only tests produce extended periods of steady MLR, consistent with the description of steady-state burning that is limited by heat transfer through a thickening char layer [60]. Using wood dimensions and densities, we infer charring rates of 0.2-1.8 mm/min, consistent with prior literature [60]. With a constant flux, and avoiding flame feedback, pyrolysis alone yields steady heat.

The transient Phase II influences the quality of Phase III. Increased MLR in the presence of a flame causes more rapid depletion of the fuel, such that piloted-ignition tests are complete well before pyrolysis-only tests. A longer period of steady-state operation might occur with thicker samples, but many of the ignition tests never show a flat Phase III. The coupling between MLR, gas-phase heat release, and radiative feedback may explain these steady, sharp declines. These declining MLRs are not the onset of extinction (Phase IV) but proceed for several minutes. Thus, allowing flame feedback depletes the matrix of pyrolyzate, limiting the release rates and steady burning in Phase III.

Although flame behavior in Phase II is not the target of this analysis, we observe that the absolute increases above pyrolytic baseline has a similar magnitude for all heat fluxes and woods.

The mass released during Phase II can cause fuel-rich burning conditions and a soot producing diffusion flame.

A distinction that appears near the end of Phase III is a brief rise in MLR under some conditions, which is particularly common when rapid heat transfer is possible. Figure 24 shows this phenomenon, beginning at 1600 s, for white oak in the *LGz* orientation where heat flux travels along the conductive grain. MLR for Douglas fir also appears in the figure. Although the two woods show a nearly identical peak mass loss near 1100 s, the second peak does not appear in Douglas fir, a softwood. We attribute this phenomenon to the thermal wave reaching the outer boundary of the material, leaving heat to accelerate reactions within the wood. Fawaz *et al.* [53] measured and modeled similar secondary peaks in samples with heat applied symmetrically from both sides. The occurrence of such a peak would depend on the sample thickness and heat transfer rate.

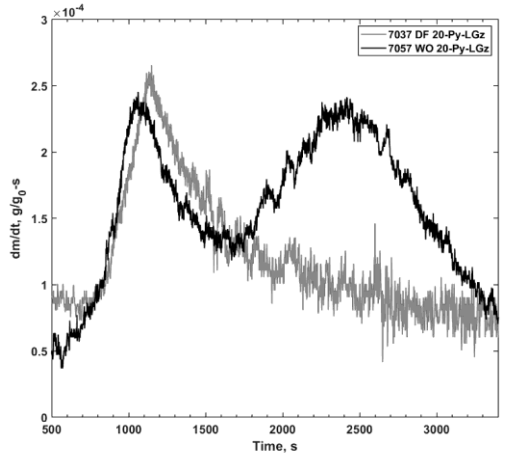

Figure 24. Pyrolysis mass loss rate profiles for Douglas fir (grey) and white oak (black) at 20 kW m-2 in *LGz* grain orientation.

In summary, the most useful Phase III would have steady MLR, which is achieved with a constant applied heat flux. The transient Phase II peak depletes the matrix of fuel and may create

soot producing conditions and should be minimized when possible. Flame feedback to the burning solid also adds variability and rapid decline in MLR. Separation of heat generated in the gas phase from the heat needed for pyrolysis may yield steady heat production and stable, low-emitting flames.

6.5 Conclusions

The aim of this work is to utilize deliberate combustion methodologies to identify what phases of burning should receive additional focus to contribute to solving the problem of human smoke exposure. We defined phases of burning based on association with periods of high exposure risk. The goal of this paper was to identify conditions that lead to a high risk of human exposure, and to identify remedies for those conditions.

Burning phases were identified associated with burning events that run a high risk of PM release. A Phase I borderline condition at 15 kW m^{-2} was identified by the observation that ignition is highly dependent on grain orientation at this heat flux. Ignition energy ratio (IER) was compared to heat flux for different wood types which showed that 30 kW m^{-2} is a valuable target for reducing the amount of energy required to achieve ignition.

Results from pyrolysis tests showed that steady-constant mass loss is possible during Phase III. Pyrolysis-only tests show mass release at 40 kW m^{-2} meet ideal cooking conditions compared to MLR at 20 kW m^{-2}. The effect of flame feedback shows a rapid consumption of fuel, preventing release patterns observed in pyrolysis tests. Redirection of radiative feedback away from the sample may cause release to more closely resemble pyrolysis mass loss.

Chapter 7

Conclusions, contributions, and future work

This chapter contains a summary of results from Chapters 4, 5, and 6. Contributions are highlighted as they apply to the research objectives for this work. Finally, recommended future work is discussed.

7.1 Conclusions

In this work I show the linkage of burning mechanisms to the release of PM. This involves the curation of language and communication tools that enable the dissemination of findings to the fire science and aerosol science communities. The development of language in Chapter 4 encompassed by "deliberate combustion" and burning phases which communicate stages of burning associated with high exposure risk were used to label needs in the stove community to fire journals. Ignition factors identified from experiments utilizing variable heat flux and wood orientations resulted in the concept of "pyrolytic acceleration" which is determined to be a necessary precursor to ignition. Particle data is used to show PM release prior to pyrolytic acceleration. Borderline conditions for reducing PM release are identified and recommendations are provided to aid in avoiding unfavorable stove operation. Conclusions from these findings are expanded on here, followed by a summary of my contributions.

In Chapter 4 I presented experiments designed to invoke causes of variation in real-world wood and assessed experiments in the context of deliberate combustion. When wood grain is aligned with heat flux at 30 and 40 kW m^{-2} time to pyrolysis is slower. Time to pyrolytic

acceleration and ignition for different woods was shown to have a relationship with external heat flux but not with thermal inertia determined from wood properties; an unexpected finding.

I showed that heat flux controls pyrolytic acceleration and the subsequent ignition of wood more than altering material properties. I demonstrated through a simple but extensive set of measurements that current ignition prediction capabilities do not conform to a well-accepted theory. This level of predictability was identified to still be useful for designers of deliberate combustion devices. The use of fire science principles demonstrated for deliberate combustion in this work shows that some development is required to understand the relationship between pre-ignition pyrolysis and deliberate ignition.

In Chapter 5 I reported an expanded characterization of fire-science experiments used to identify how particulate matter is released prior to ignition of thermally-thick solid fuel. This work identifies a burning mechanism that releases small nucleation particles first, then particle mass increases, before giving way to another reaction that generates both CO and condensable material. This mechanism was identified using aerosol measurements coupled with mass loss rate and CO and CO_2 emissions data. Recognizing the need for minimum heat flux and the influence of orientation supports practical guidance for reducing the exposure of stove users.

In Chapter 6 I compiled experimental findings which were used to assess ideal burning conditions contributing to target objectives. This work identified phases of burning that require additional focus for solving problems related to human exposure by associating features of mass loss to undesirable stove operation conditions. 15 kW m^{-2} represents a heat-based borderline condition which I recommend avoiding due to prolonged ignition times and grain-dependent flammability. Phase III release patterns should be steady and long in duration, which is compromised by flame feedback effects.

7.2 Contributions

Contributions reported here result from the accomplishment of the four stated objectives of this project. **Objective 1** was to identify necessary language and frameworks to communicate needs from the cook stoves research field to fire science engineers for reducing PM pollution. In the context of fire safety engineering which aims to prevent ignition, the term "deliberate combustion" was defined. Language frameworks associated with the use of fire science principles describe the intentional creation of fire for the reduction of a pollutant (Chapter 4). This work supports necessary communication of needs to an uninitiated discipline. This effort includes development of the concept of burning phases that specify stages of burning that are associated with high exposure risk for stove users (Chapters 4 and 6).

Objective 2 was to experimentally isolate limiting factors for controlling ignition that aims to reduce energy demand and PM release. An experimental campaign was developed which systematically investigated the effects of material properties, heating conditions, and flammability, totaling 111 experiments. This objective was achieved by identifying a fundamental phenomenon I call *pyrolytic acceleration* (Chapter 4). This metric was shown to be a necessary precursor to ignition and provided context for further research objectives. A metric of ignition energy ratio (IER) was developed which quantifies the ratio of energy required for ignition to the energy produced from complete combustion. This metric was used to conclude that wood properties do not significantly alter IER but that heat flux does decrease IER (Chapter 4).

Objective 3 was to experimentally characterize pre-ignition PM release associated with ignition limitation factors. A series of experiments were performed which coupled aerosol sampling methodology to classic fire science experimentation techniques. A total of 55 hours of

low heat flux experiments were conducted, resulting from 34 trials. This objective was achieved by describing a previously unidentified burning phenomena in which nucleation mode particulate matter is released prior to pyrolytic acceleration (Chapter 5). This was confirmed from coordinating particle measurements with mass loss rates and CO and CO_2 emission measurements.

Objective 4 was to identify guidelines for ideal burning using ignition and PM release factors identified from experimentation to provide recommendations for exposure reduction. This objective was achieved first by associating burning events that run a high risk of PM release. A Phase I borderline condition at 15 kW m^{-2} was identified by demonstrating that ignition at this heat flux is highly dependent on grain orientation. Ignition energy ratio (IER) was compared to heat flux for different wood types showing that 30 kW m^{-2} is a recommended target for reducing the amount of ignition energy required. Pyrolysis tests showed that steady-constant mass loss is ideal for Phase III burning. Pyrolysis-only tests show mass release patterns at 40 kW m^{-2} are ideal for cooking use compared to MLR at 20 kW m^{-2}. Flame feedback was shown to rapidly consume fuel, preventing release slow patterns identified as ideal in pyrolysis tests. Redirection of radiative feedback away from the sample may cause release to more closely resemble pyrolysis mass loss.

7.3 Future work

Current ignition theory is limited in capabilities that inform prediction of where mass can be expected to release on a single piece of wood and how ignition at the localized site should occur. Additionally, findings derived from "ideal-world" laboratory measurements are limited in their use for fully developing a burning protocol to reduce $PM_{2.5}$. Continued work should expand understanding of mass transfer limitations and confirmation of theory developed herein for real-world settings. Future research suggestions are described in the sections that follow.

7.3.1 Combustion mechanisms

Low heat flux ignition: Ignition is well understood to be a heat-driven process [56]. Findings reported here confirm the most effective way of reducing energy requirements for ignition and reducing PM release is by increasing the initial heat delivery to the sample. However, results shown in Chapters 5 and 6 at 15 kW m^{-2} indicate that mass transfer in the *LGx* and *LGz* grain orientations play a larger role in the pyrolytic acceleration event. Accelerated mass loss and subsequent ignition observed for *LGz* during conditions which cause *LGx* to release mass at a constant and slow rate suggests mass may be trapped in the char layer or unable to escape. Understanding the behavior of mass transfer at low heat flux will clarify factors controlling ignition when ignition energy ratios are high.

Spatial release: The primary method of reducing PM utilized in this work necessitates the passage of PM-forming tars through an existing flame. Findings reported here assume gas-phase mixing is thorough and, when piloted, representative mass loss is consumed by a flame. However, gas-phase mixing in a real-world setting is not well understood. Morrisset *et al.* describe the extinction of localized flamelets when mass loss rate goes below critical values for sustaining a flame [137]. Flamelet extinction is representative of exposure sources in real-world burning. Ensuring PM released from an extinguished portion of char passes through a flame is possible if mass transfer mechanisms are more fully understood.

7.3.2 Real-world burning

Practical methods of burning are difficult to study in the laboratory setting due to the difficulty of constraining variables in the field. Work presented here aims to reveal heat and mass transfer mechanisms that can lead to faster ignition and the passage of pyrolysis products through a flame. Extrapolation of these methods to real-world burning protocols requires assessment of how to translate developed theory to practical stove operation techniques. In real-world stove operation multiple units of fuel are used to increase heat output. Variables like volatile mass interchange between logs, radiation from kindling and tinder to large logs, and stove design with user-initiated fuel maneuvers all represent challenges to implementation. Understanding fire science fundamentals in a real-world setting requires additional focus on these, and other variables.

The use of curated laboratory prepared samples to assess ignition conditions and burning mechanisms is not intended to replicate user-experience. In real-world burning conditions fuel contains bark, knots, sap deposits, and variable moisture content. Features like bark and moisture cause an increase time to ignition, while wood charred in previous fire will decrease time to ignition. Experimentation utilized in the assessment of fire science principles applied to reducing PM release required predictable fuel behavior with known and comparable geometries, free of imperfections. When heat flux and exposed end grain conditions are replicated the results shown here are transferrable to real-world fuel types. This is reliable since these principles were developed with naturally occurring anatomical features of wood which are present in any wood species. For example, application of sufficient heat to any wood type containing imperfections will result in pyrolytic acceleration and the production of ignitable fuel. The ignition energy ratio is a useful metric for prescribing the necessary heat flux for reducing energy demand and minimizing time to ignition. However, we expect differences in these results to be observed when additional

heat sinks are present. Thick and thin bark, low and high moisture content, and localized imperfections with low and high densities represent some causes of increased PM release which consume variable amounts of heat otherwise utilized to achieve pyrolytic acceleration. Future work is recommended to characterize how much variables like these increase time to pyrolytic acceleration.

Efficient heat generated by kindling and tinder and the heat required for ignition determines stove-user ability to achieve low IERs. To ensure a pyrolytic acceleration event occurs heat delivery from kindling and tinder should be studied further since work reported here can only inform ignition of large wood given efficient heat transfer. Effects of fuel size, quantity of heat flux delivered to the wood from the firebox, and control of flame feedback are all uncharacterized factors controlling ignition and PM reduction. An additional area of focus in fire starting materials would answer questions related to the generation of 30 kW m^{-2} from tinder and kindling.

7.4 Summary

To summarize this work, heat and mass transfer fundamentals developed for use in fire safety engineering were employed to achieve deliberate combustion of wood for the reduction of a pollutant, $PM_{2.5}$. This work improves upon foundational knowledge required to solve the problem of human exposure in the cooking environment.

REFERENCES

[1] IEA, IRENA, UNSD, World Bank, WHO, Tracking SDG 7: The Energy Progress Report 2021, (2021).

[2] S.S. Lim, et al., A comparative risk assessment of burden of disease and injury attributable to 67 risk factors and risk factor clusters in 21 regions, 1990–2010: a systematic analysis for the Global Burden of Disease Study 2010, The Lancet 380 (2012) 2224–2260. https://doi.org/https://doi.org/10.1016/S0140-6736(12)61766-8.

[3] T.C. Bond, D.G. Streets, K.F. Yarber, S.M. Nelson, J.H. Woo, Z. Klimont, A technology-based global inventory of black and organic carbon emissions from combustion, Journal of Geophysical Research: Atmospheres 109 (2004) 1–43. https://doi.org/10.1029/2003JD003697.

[4] T.C. Bond, Z. Merrin, Appliances for Cooking, Heating, and Other Energy Services, in: Handbook of Indoor Air Quality, Springer, 2022: pp. 1–36.

[5] M. Ezzati, D.M. Kammen, The health impacts of exposure to indoor air pollution from solid fuels in developing countries: Knowledge, gaps, and data needs, Environ. Health Perspect. 110 (2002) 1057–1068. https://doi.org/10.1289/ehp.021101057.

[6] O.P. Kurmi, S. Semple, P. Simkhada, W. Cairns S Smith, J.G. Ayres, COPD and chronic bronchitis risk of indoor air pollution from solid fuel: A systematic review and meta-analysis, Thorax 65 (2010) 221–228. https://doi.org/10.1136/thx.2009.124644.

[7] O. Stoner, J. Lewis, I.L. Martínez, S. Gumy, T. Economou, H. Adair-Rohani, Household cooking fuel estimates at global and country level for 1990 to 2030, Nat. Commun. 12 (2021). https://doi.org/10.1038/s41467-021-26036-x.

[8] R.J. Thompson, J. Li, C.L. Weyant, R. Edwards, Q. Lan, N. Rothman, W. Hu, J. Dang, A. Dang, K.R. Smith, T.C. Bond, Field Emission Measurements of Solid Fuel Stoves in Yunnan, China Demonstrate Dominant Causes of Uncertainty in Household Emission Inventories, Environ. Sci. Technol. 53 (2019) 3323–3330. https://doi.org/10.1021/acs.est.8b07040.

[9] X. Li, S. Clark, E. Floess, J. Baumgartner, T. Bond, E. Carter, Personal exposure to PM2.5 of indoor and outdoor origin in two neighboring Chinese communities with contrasting household fuel use patterns, Science of the Total Environment 800 (2021). https://doi.org/10.1016/j.scitotenv.2021.149421.

[10] M. Shupler, W. Godwin, J. Frostad, P. Gustafson, R.E. Arku, M. Brauer, Global estimation of exposure to fine particulate matter (PM2.5) from household air pollution, Environ. Int. 120 (2018) 354–363. https://doi.org/10.1016/j.envint.2018.08.026.

[11] S. Batliwala, Women and Cooking Energy, Econ. Polit. Wkly. 18 (1983) 2227–2230.

[12] T.C. Bond, D.G. Streets, K.F. Yarber, S.M. Nelson, J.H. Woo, Z. Klimont, A technology-based global inventory of black and organic carbon emissions from combustion, Journal of Geophysical Research: Atmospheres 109 (2004). https://doi.org/10.1029/2003JD003697.

[13] C.A. Roden, T.C. Bond, S. Conway, A.B. Osorto Pinel, Emission factors and real-time optical properties of particles emitted from traditional wood burning cookstoves, Environ. Sci. Technol. 40 (2006) 6750–6757. https://doi.org/10.1021/es052080i.

[14] A.P. Grieshop, J.D. Marshall, M. Kandlikar, Health and climate benefits of cookstove replacement options, Energy Policy 39 (2011) 7530–7542. https://doi.org/10.1016/j.enpol.2011.03.024.

[15] R. Quansah, S. Semple, C.A. Ochieng, S. Juvekar, F.A. Armah, I. Luginaah, J. Emina, Effectiveness of interventions to reduce household air pollution and/or improve health in homes using solid fuel in low-and-middle income countries: A systematic review and meta-analysis, Environ. Int. 103 (2017) 73–90. https://doi.org/10.1016/j.envint.2017.03.010.

[16] E.A. Brakema, R.M. van der Kleij, D. Vermond, F.A. van Gemert, B. Kirenga, N.H. Chavannes, P. Le An, M. Anastasaki, A. Akylbekov, A. Barton, A. Bertsias, P.D.U. Binh, J.F.M. van Boven, D. Burges, L. Cartwright, V.E. Chatzea, L. Cragg, T.N. Dang, I. Dautov, B. Emilov, I. Ferarrio, B. Hedrick, L.H. Thi Cam Hong, N. Hopkinson, E. Isaeva, R. Jones, C. de Jong, S. van Kampen, W. Katagira, J. Kjærgaard, J. Kocks, L.T.T. Lan, T.T.D. Linh, C. Lionis, K.X. Loan, M. Mademilov, A. McEwen, P. Musinguzi, R. Nantanda, G. Ndeezi, S. Papadakis, H. Pinnock, J. Pooler, C.C. Poot, M.J. Postma, A. Poulsen, P. Powell, N.N. Quynh, S. Reventlow, D. Sifaki-Pistolla, S. Singh, T. Sooronbaev, J. Correia de Sousa, J. Stout, M. Stubbe Østergaard, A. Tabyshova, I. Tsiligianni, T.D. Tuan, J. Tumwine, L.T. Van, N.N. Vinh, S. Walusimbi, L. Warren, S. Williams, Let's stop dumping cookstoves in local communities. It's time to get implementation right, NPJ Prim. Care Respir. Med. 30 (2020). https://doi.org/10.1038/s41533-019-0160-8.

[17] E. Phillip, J. Langevin, M. Davis, N. Kumar, A. Walsh, V. Jumbe, M. Clifford, R. Conroy, D. Stanistreet, Improved cookstoves to reduce household air pollution exposure in sub-Saharan Africa: A scoping review of intervention studies, PloS One 18 (2023). https://doi.org/10.1371/journal.pone.0284908.

[18] O. Masera, R. Edwards, C. Armendáriz Arnez, V. Berrueta, M. Johnson, L. Rojas Bracho, H. Riojas-Rodríguez, K.R. Smith, Impact of Patsari improved cookstoves on indoor air quality in Michoacán, Mexico, 2007.

[19] R. Bailis, V. Berrueta, C. Chengappa, K. Dutta, R. Edwards, O. Masera, D. Still, K.R. Smith, Performance testing for monitoring improved biomass stove interventions: experiences of the Household Energy and Health Project, Energy for Sustainable Development 11 (2007) 57–70. https://doi.org/10.1016/S0973-0826(08)60400-7.

[20] C. Chengappa, R. Edwards, R. Bajpai, K.N. Shields, K.R. Smith, Impact of improved cookstoves on indoor air quality in the Bundelkhand region in India, Energy for Sustainable Development 11 (2007) 33–44. https://doi.org/10.1016/S0973-0826(08)60398-1.

[21] C.A. Roden, T.C. Bond, S. Conway, A.B. Osorto Pinel, N. MacCarty, D. Still, Laboratory and field investigations of particulate and carbon monoxide emissions from traditional and improved cookstoves, Atmos. Environ. 43 (2009) 1170–1181. https://doi.org/10.1016/j.atmosenv.2008.05.041.

[22] C. Boman, A. Nordin, M. Öhman, D. Boström, R. Westerholm, Emissions from small-scale combustion of biomass fuels-extensive quantification and characterization, 2005.

[23] E.M. Carter, M. Shan, X. Yang, J. Li, J. Baumgartner, Pollutant emissions and energy efficiency of iresaf gasifier cooking stoves and implications for future intervention studies, Environ. Sci. Technol. 48 (2014) 6461–6467. https://doi.org/10.1021/es405723w.

[24] A. Kocbach Bølling, J. Pagels, K.E. Yttri, L. Barregard, G. Sallsten, P.E. Schwarze, C. Boman, Health effects of residential wood smoke particles: the importance of combustion conditions and physicochemical particle properties, Part. Fibre Toxicol. 6 (2009). https://doi.org/10.1186/1743-8977-6-29.

[25] Y. Chen, C.A. Roden, T.C. Bond, Characterizing biofuel combustion with Patterns of Real-Time Emission Data (PaRTED), Environ. Sci. Technol. 46 (2012) 6110–6117. https://doi.org/10.1021/es3003348.

[26] J. Zalzal, Y. Liu, A. Smargiassi, M. Hatzopoulou, Improving residential wood burning emission inventories with the integration of readily available data sources, Science of the Total Environment 946 (2024). https://doi.org/10.1016/j.scitotenv.2024.174226.

[27] T. Wolf, L.H. Pettersson, I. Esau, Dispersion of particulate matter (PM2.5) from wood combustion for residential heating: Optimization of mitigation actions based on large-eddy simulations, Atmos. Chem. Phys. 21 (2021) 12463–12477. https://doi.org/10.5194/acp-21-12463-2021.

[28] L.P. Naeher, M. Brauer, M. Lipsett, J.T. Zelikoff, C.D. Simpson, J.Q. Koenig, K.R. Smith, Woodsmoke health effects: A review, Inhal. Toxicol. 19 (2007) 67–106. https://doi.org/10.1080/08958370600985875.

[29] J. Burkhardt, J. Bayham, A. Wilson, E. Carter, J.D. Berman, K. O'Dell, B. Ford, E. V Fischer, J.R. Pierce, The effect of pollution on crime : Evidence from data on particulate matter and ozone, J. Environ. Econ. Manage. 98 (2019) 102267. https://doi.org/10.1016/j.jeem.2019.102267.

[30] A. Dearden, Y. He, A. Akherati, C.Y. Lim, M.M. Coggon, A.R. Koss, J. de Gouw, C. Warneke, L.D. Yee, J.H. Seinfeld, C.D. Cappa, J.H. Kroll, J.R. Pierce, S.H. Jathar, Multi-day photochemical evolution of organic aerosol from biomass burning emissions, Environmental Science: Atmospheres 4 (2024) 925–941. https://doi.org/10.1039/d3ea00111c.

[31] A.M. Avery, M. Fawaz, L.R. Williams, T. Bond, T.B. Onasch, Chemically distinct particle-phase emissions from highly controlled pyrolysis of three wood types, Atmos. Chem. Phys. 23 (2023) 8837–8854. https://doi.org/10.5194/acp-23-8837-2023.

[32] A.C. Eriksson, E.Z. Nordin, R. Nyström, E. Pettersson, E. Swietlicki, C. Bergvall, R. Westerholm, C. Boman, J.H. Pagels, Particulate PAH emissions from residential biomass combustion: Time-resolved analysis with aerosol mass spectrometry, Environ. Sci. Technol. 48 (2014) 7143–7150. https://doi.org/10.1021/es500486j.

[33] K.R. Bilsback, J. Dahlke, K.M. Fedak, N. Good, A. Hecobian, P. Herckes, C. L'Orange, J. Mehaffy, A. Sullivan, J. Tryner, L. Van Zyl, E.S. Walker, Y. Zhou, J.R. Pierce, A. Wilson, J.L. Peel, J. Volckens, A Laboratory Assessment of 120 Air Pollutant Emissions from Biomass and Fossil Fuel Cookstoves, Environ. Sci. Technol. 53 (2019) 7114–7125. https://doi.org/10.1021/acs.est.8b07019.

[34] J.R. Odum, T. Hoffmann, F. Bowman, D. Collins, R.C. Flagan, J.H. Seinfeld, Gas/particle partitioning and secondary organic aerosol yields, Environ. Sci. Technol. 30 (1996) 2580–2585. https://doi.org/10.1021/es950943+.

[35] M. Hallquist, J.C. Wenger, U. Baltensperger, Y. Rudich, D. Simpson, M. Claeys, J. Dommen, N.M. Donahue, C. George, A.H. Goldstein, J.F. Hamilton, H. Herrmann, T. Hoffmann, Y. Iinuma, M. Jang, M.E. Jenkin, J.L. Jimenez, A. Kiendler-Scharr, W. Maenhaut, G. McFiggans, T.F. Mentel, A. Monod, A.S.H. Prévôt, J.H. Seinfeld, J.D. Surratt, R. Szmigielski, J. Wildt, The formation, properties and impact of secondary organic aerosol: Current and emerging issues, Atmos. Chem. Phys. 9 (2009) 5155–5236. https://doi.org/10.5194/acp-9-5155-2009.

[36] G. Stefenelli, J. Jiang, A. Bertrand, E.A. Bruns, S.M. Pieber, U. Baltensperger, N. Marchand, S. Aksoyoglu, A.S.H. Prévôt, J.G. Slowik, I. El Haddad, Secondary organic aerosol formation from smoldering and flaming combustion of biomass: A box model

parametrization based on volatility basis set, Atmos. Chem. Phys. 19 (2019) 11461–11484. https://doi.org/10.5194/acp-19-11461-2019.

[37] A.P. Grieshop, J.M. Logue, N.M. Donahue, A.L. Robinson, Laboratory investigation of photochemical oxidation of organic aerosol from wood fires 1: Measurement and simulation of organic aerosol evolution, Atmos. Chem. Phys. 9 (2009) 1263–1277. https://doi.org/10.5194/acp-9-1263-2009.

[38] A.P. Grieshop, N.M. Donahue, A.L. Robinson, Laboratory investigation of photochemical oxidation of organic aerosol from wood fires 2: Analysis of aerosol mass spectrometer data, Atmos. Chem. Phys. 9 (2009) 2227–2240. https://doi.org/10.5194/acp-9-2227-2009.

[39] A.P. Grieshop, M.A. Miracolo, N.M. Donahue, A.L. Robinson, Constraining the volatility distribution and gas-particle partitioning of combustion aerosols using isothermal dilution and thermodenuder measurements, Environ. Sci. Technol. 43 (2009) 4750–4756. https://doi.org/10.1021/es8032378.

[40] A.L. Hodshire, A. Akherati, M.J. Alvarado, B. Brown-Steiner, S.H. Jathar, J.L. Jimenez, S.M. Kreidenweis, C.R. Lonsdale, T.B. Onasch, A.M. Ortega, J.R. Pierce, Aging Effects on Biomass Burning Aerosol Mass and Composition: A Critical Review of Field and Laboratory Studies, Environ. Sci. Technol. 53 (2019) 10007–10022. https://doi.org/10.1021/acs.est.9b02588.

[41] X. Zhang, C.D. Cappa, S.H. Jathar, R.C. McVay, J.J. Ensberg, M.J. Kleeman, J.H. Seinfeld, Influence of vapor wall loss in laboratory chambers on yields of secondary organic aerosol, Proc. Natl. Acad. Sci. U. S. A. 111 (2014) 5802–5807. https://doi.org/10.1073/pnas.1404727111.

[42] J.I. Lachowicz, S. Milia, M. Jaremko, E. Oddone, E. Cannizzaro, L. Cirrincione, G. Malta, M. Campagna, L.I. Lecca, Cooking Particulate Matter: A Systematic Review on Nanoparticle Exposure in the Indoor Cooking Environment, Atmosphere (Basel). 14 (2023). https://doi.org/10.3390/atmos14010012.

[43] R.E. Arku, A. Birch, M. Shupler, S. Yusuf, P. Hystad, M. Brauer, Characterizing exposure to household air pollution within the Prospective Urban Rural Epidemiology (PURE) study, Environ. Int. 114 (2018) 307–317. https://doi.org/10.1016/j.envint.2018.02.033.

[44] M. Fawaz, A. Avery, L. Williams, T. Onasch, T.C. Bond, A study of governing factors of organic aerosol emissions during controlled wood pyrolysis experiments, (2020).

[45] S.L. Haslett, J.C. Thomas, W.T. Morgan, R. Hadden, D. Liu, J.D. Allan, P.I. Williams, S. Keita, C. Liousse, H. Coe, Highly controlled, reproducible measurements of aerosol emissions from combustion of a common African biofuel source, Atmos. Chem. Phys. 18 (2018) 385–403. https://doi.org/10.5194/acp-18-385-2018.

[46] J.S. Reid, R. Koppmann, T.F. Eck, D.P. Eleuterio, A review of biomass burning emissions part II: intensive physical properties of biomass burning particles, 2005. www.atmos-chem-phys.org/acp/5/799/Sref-ID:1680-7324/acp/2005-5-799EuropeanGeosciencesUnion.

[47] Z. Ning, C. Sioutas, Atmospheric processes influencing aerosols generated by combustion and the inference of their impact on public exposure: A review, Aerosol Air Qual. Res. 10 (2010) 43–58. https://doi.org/10.4209/aaqr.2009.05.0036.

[48] M. Obaidullah, S. Bram, V.K. Verma, J. De Ruyck, A Review on Particle Emissions from Small Scale Biomass Combustion, 2 (2012).

[49] J. Chen, C. Li, Z. Ristovski, A. Milic, Y. Gu, M.S. Islam, S. Wang, J. Hao, H. Zhang, C. He, H. Guo, H. Fu, B. Miljevic, L. Morawska, P. Thai, Y.F. LAM, G. Pereira, A. Ding, X.

Huang, U.C. Dumka, A review of biomass burning: Emissions and impacts on air quality, health and climate in China, Science of the Total Environment 579 (2017) 1000–1034. https://doi.org/10.1016/j.scitotenv.2016.11.025.

[50] M. Elsasser, C. Busch, J. Orasche, C. Schön, H. Hartmann, J. Schnelle-Kreis, R. Zimmermann, Dynamic changes of the aerosol composition and concentration during different burning phases of wood combustion, Energy and Fuels 27 (2013) 4959–4968. https://doi.org/10.1021/ef400684f.

[51] Y. Chen, C.A. Roden, T.C. Bond, Characterizing biofuel combustion with Patterns of Real-Time Emission Data (PaRTED), Environ. Sci. Technol. 46 (2012) 6110–6117. https://doi.org/10.1021/es3003348.

[52] M. Fawaz, C. Lautenberger, T.C. Bond, Prediction of organic aerosol precursor emission from the pyrolysis of thermally thick wood, Fuel 269 (2020). https://doi.org/10.1016/j.fuel.2020.117333.

[53] M. Fawaz, A. Avery, T.B. Onasch, L.R. Williams, T.C. Bond, Technical note: Pyrolysis principles explain time-resolved organic aerosol release from biomass burning, Atmos. Chem. Phys. 21 (2021) 15605–15618. https://doi.org/10.5194/acp-21-15605-2021.

[54] A. Atreya, Ignition of Fires, Philosophical Transactions: Mathematical, Physical and Engineering Sciences 356 (1998) 2787–2813. https://about.jstor.org/terms.

[55] V. Babrauskas, Ignition handbook: principles and applications to fire safety engineering, fire investigation, risk management and forensic science, 2014.

[56] D.D. Drysdale, Ignition: The Initiation of Flaming Combustion, in: An Introduction to Fire Dynamics, Third Edit, John Wiley & Sons, Ltd., 2011: pp. 225–276.

[57] J.L. Torero, Flaming Ignition of Solid Fuels, in: SFPE Handbook of Fire Protection Engineering, Springer US, New York City, NY, 2016: pp. 633–661.

[58] V. Babrauskas, Ignition of wood: A review of the state of the art, Journal of Fire Protection Engineering 12 (2002) 163–189. https://doi.org/10.1177/10423910260620482.

[59] D. Drysdale, An introduction to fire dynamics, Third Ed, John Wiley & Sons, Scotland, 2011.

[60] A.I. Bartlett, R.M. Hadden, L.A. Bisby, A Review of Factors Affecting the Burning Behaviour of Wood for Application to Tall Timber Construction, Fire Technol. 55 (2019). https://doi.org/10.1007/s10694-018-0787-y.

[61] N.M. Donahue, A.L. Robinson, C.O. Stanier, S.N. Pandis, Coupled partitioning, dilution, and chemical aging of semivolatile organics, Environ. Sci. Technol. 40 (2006) 2635–2643. https://doi.org/10.1021/es052297c.

[62] R. Emberley, A. Inghelbrecht, Z. Yu, J.L. Torero, Self-extinction of timber, Proceedings of the Combustion Institute 36 (2017) 3055–3062. https://doi.org/10.1016/j.proci.2016.07.077.

[63] R. Emberley, T. Do, J. Yim, J.L. Torero, Critical heat flux and mass loss rate for extinction of flaming combustion of timber, Fire Saf. J. 91 (2017) 252–258. https://doi.org/10.1016/j.firesaf.2017.03.008.

[64] S. McAllister, Critical mass flux for flaming ignition of wet wood, Fire Saf. J. 61 (2013) 200–206. https://doi.org/10.1016/j.firesaf.2013.09.002.

[65] M.J. Hurley, D. Gottuk, J.R. Hall, K. Harada, E. Kuligowski, M. Puchovsky, J.L. Torero, J.M. Watts, C. Wieczorek, eds., SFPE Handbook of Fire Protection Engineering, Fifth, Springer, New York City, 2016.

[66] S.I. Stoliarov, Y. Ding, Pyrolysis model parameterization and fire growth prediction: The state of the art, Fire Saf. J. 140 (2023). https://doi.org/10.1016/j.firesaf.2023.103905.

[67] C. Lautenberger, C. Fernandez-Pello, Generalized pyrolysis model for combustible solids, Fire Saf. J. 44 (2009) 819–839. https://doi.org/10.1016/j.firesaf.2009.03.011.

[68] X. Lu, X. Gu, A review on lignin pyrolysis: pyrolytic behavior, mechanism, and relevant upgrading for improving process efficiency, Biotechnology for Biofuels and Bioproducts 15 (2022). https://doi.org/10.1186/s13068-022-02203-0.

[69] R.C. Pettersen, The Chemical Composition of Wood, n.d.

[70] C. Di Blasi, Modeling chemical and physical processes of wood and biomass pyrolysis, Prog. Energy Combust. Sci. 34 (2008) 47–90. https://doi.org/10.1016/j.pecs.2006.12.001.

[71] E. Syguła, D. Ciolkosz, A. Białowiec, The significance of structural components of lignocellulosic biomass on volatile organic compounds presence on biochar – a review, Wood Sci. Technol. 58 (2024) 859–886. https://doi.org/10.1007/s00226-024-01557-y.

[72] D. Shen, R. Xiao, S. Gu, K. Luo, The pyrolytic behavior of cellulose in lignocellulosic biomass: A review, RSC Adv. 1 (2011) 1641–1660. https://doi.org/10.1039/c1ra00534k.

[73] H.W. Emmons, The Further History of F re Science, Gordon and Breach Science Publishers, 1984.

[74] D.B. Spalding, The Combustion of Liquid Fuels, Nature (1953) 847–864.

[75] D.B. Spalding, A Theory of Inflammability Limits and Flame-Quenching, Proc. R. Soc. Lond. A Math. Phys. Sci. 240 (1957) 83–100. https://www.jstor.org/stable/100160.

[76] H.W. Emmons, The film combustion of liquid fuel, Z. Angew. Math. Mech. 36 (1956) 60–71.

[77] D.J. Rasbash, The relevance of firepoint theory to the assessment of the fire behavior of combustible materials, in: International Symposium on Fire Safety of Combustible Materials, Edinburgh University, 1975: pp. 169–178.

[78] D.J. Rasbash, D.D. Drysdale, D. Deepak, Critical heat and mass transfer at pilot ignition and extinction of a material, Fire Saf. J. 10 (1986) 1–10. https://doi.org/10.1016/0379-7112(86)90026-3.

[79] D.D. Drysdale, H.E. Thomson, Flammability of plastics II: Critical mass flux at the firepoint, Fire Saf. J. 14 (1989) 179–188. https://doi.org/10.1016/0379-7112(89)90071-4.

[80] A. Tewarson, J.L. Lee, R.F. Pion, THE INFLUENCE OF OXYGEN CONCENTRATION ON FUEL PARAMETERS FOR FIRE MODELING, 1981.

[81] A. Tewarson, R.F. Pion, Flammability of PlasticsmI. Burning Intensity, 1976.

[82] A. Tewarson, R.F. Pion, Burning Intensity of Commercial Samples of Plastics, Fire Technol. 11 (1975) 274–281.

[83] A. Tewarson, Heat release rate in fires, Fire Mater. 4 (1980) 185–191. https://doi.org/10.1002/fam.810040405.

[84] M. Janssens, A thermal model for piloted ignition of wood including variable thermophysical properties, Fire Safety Science: Proceedings of the Third International Symposium (1991) 167–176. https://doi.org/10.4324/9780203973493.

[85] M. Janssens, Rate of heat release of wood products, Fire Saf. J. 17 (1991) 217–238. https://doi.org/10.1016/0379-7112(91)90003-H.

[86] M.L. Janssens, Measuring rate of heat release by oxygen consumption, Fire Technol. 27 (1991) 234–249. https://doi.org/10.1007/BF01038449.

[87] M.J. Spearpoint, J.G. Quintiere, Predicting the piloted ignition of wood in the cone calorimeter using an integral model – Effect of species, grain orientation and heat flux, Fire Saf. J. 36 (2001) 391–415. https://doi.org/10.1016/S0379-7112(00)00055-2.

[88] N. Boonmee, J.G. Quintiere, Glowing ignition of wood: The onset of surface combustion, Proceedings of the Combustion Institute 30 II (2005) 2303–2310. https://doi.org/10.1016/j.proci.2004.07.022.

[89] A. Fernandez-Pello, F.A. Williams, A Theory of Laminar Flame Spread Over Flat Surfaces of Solid Combustibles, 1977.

[90] D. Rich, C. Lautenberger, J.L. Torero, J.G. Quintiere, C. Fernandez-Pello, Mass flux of combustible solids at piloted ignition, Proceedings of the Combustion Institute 31 II (2007) 2653–2660. https://doi.org/10.1016/j.proci.2006.08.055.

[91] C. Di Blasi, Heat, momentum and mass transport through a shrinking biomass particle exposed to thermal radiation, Chem. Eng. Sci. 51 (1996) 1121–1132. https://doi.org/10.1016/S0009-2509(96)80011-X.

[92] C. Di Blasi, A transient, two-dimensional model of biomass py- rolysis, Developments in Thermochemical Biomass Conversion (1997) 147–160.

[93] M. Janssens, Piloted Ignition of Wood: A Review, Fire Mater. 15 (1991) 151–167.

[94] Forest Products Laboratory, Wood Handbook, Wood as an Engineering Material, Madison, WI, 2010.

[95] J.F. Siau, Transport processes in wood, Springer Science & Business Media, 2012.

[96] B.M. Suleiman, J. Larfeldt, B. Leckner, M. Gustavsson, Thermal conductivity and diffusivity of wood, Wood Sci. Technol. 33 (1999) 465–473.

[97] J. Flynn, D. Morrisset, R.M. Hadden, T.C. Bond, Exploiting Wood Species and Grain Orientation to Illuminate the Onset of Pyrolysis and Ignition in Deliberate Combustion, Available at SSRN 5252657 (2025).

[98] M. Deng, S. Zhang, M. Shan, J. Li, J. Baumgartner, E. Carter, X. Yang, The impact of cookstove operation on PM2.5 and CO emissions: A comparison of laboratory and field measurements, Environmental Pollution 243 (2018) 1087–1095. https://doi.org/10.1016/j.envpol.2018.09.064.

[99] J.J. Jetter, P. Kariher, Solid-fuel household cook stoves: Characterization of performance and emissions, Biomass Bioenergy 33 (2009) 294–305. https://doi.org/10.1016/j.biombioe.2008.05.014.

[100] K.R. Bilsback, S.R. Eilenberg, N. Good, L. Heck, M. Johnson, J.K. Kodros, E.M. Lipsky, C. L'Orange, J.R. Pierce, A.L. Robinson, R. Subramanian, J. Tryner, A. Wilson, J. Volckens, The Firepower Sweep Test: A novel approach to cookstove laboratory testing, Indoor Air 28 (2018) 936–949. https://doi.org/10.1111/ina.12497.

[101] A. Galgano, C. Di Blasi, R. De Vita, Experimental Validation of a Solid-Phase Model for Wood Ignition and Burning, Energy and Fuels 32 (2018) 8494–8506. https://doi.org/10.1021/acs.energyfuels.8b01621.

[102] D. Morrisset, R.M. Hadden, A.I. Bartlett, A. Law, R. Emberley, Time dependent contribution of char oxidation and flame heat feedback on the mass loss rate of timber, Fire Saf. J. 120 (2021) 103058. https://doi.org/10.1016/j.firesaf.2020.103058.

[103] A.M. Kanury, P.L. Blackshear, Some Considerations Pertaining to the Problem of Wood-Burning, Combustion Science and Technology 1 (1970) 339–356. https://doi.org/10.1080/00102206908952214.

[104] P.M. Fine, G.R. Cass, B.R.T. Simoneit, Chemical characterization of fine particle emissions from fireplace combustion of woods grown in the northeastern United States, Environ. Sci. Technol. 35 (2001) 2665–2675. https://doi.org/10.1021/es001466k.

[105] M.A. Delichatsios, T.H. Panagiotou, F. Kiley, The Use of Time to Ignition Data for Characterizing the Thermal Inertia and the Minimum (Critical) Heat Flux for Ignition or Pyrolysis, 1991.

[106] J. Quintiere, A simplified theory for generalizing results from a radiant panel rate of flame spread apparatus, Fire Mater. 5 (1981) 52–60. https://doi.org/10.1002/fam.810050204.

[107] S.M. Dakka, G.S. Jackson, J.L. Torero, S.M. Mechanisms Dakka, Mechanisms Controlling the Degradation of Poly(methyl methacrylate) Prior to Piloted Ignition Proceedings of the Combustion Institute, 2002.

[108] C. Zhai, S. Zhang, S. Yao, Q. Zhan, S. Zhang, Y. Wang, Analytical study on ignition time of PMMA exposed to time-decreasing thermal radiation using critical mass flux, Sci. Rep. (2019) 1–12. https://doi.org/10.1038/s41598-019-48411-x.

[109] M.A. Delichatsios, Piloted ignition times, critical heat fluxes and mass loss rates at reduced oxygen atmospheres, Fire Saf. J. 40 (2005) 197–212. https://doi.org/10.1016/j.firesaf.2004.11.005.

[110] F. Richter, F.X. Jervis, X. Huang, G. Rein, Effect of oxygen on the burning rate of wood, Combust. Flame 234 (2021). https://doi.org/10.1016/j.combustflame.2021.111591.

[111] M.J. Spearpoint, J.G. Quintiere, Predicting the Burning of Wood Using an Integral Model, 2000.

[112] N. Boonmee, J.G. Quintiere, Glowing and flaming autoignition of wood, 2002.

[113] F. Vermina Plathner, P. van Hees, Experimental assessment of bench-scale ignitability parameters, Fire Mater. 43 (2019) 123–130. https://doi.org/10.1002/fam.2675.

[114] M.M. Khan, J.L. De Ris, Operator independent ignition measurements, in: Fire Safety Science, International Association for Fire Safety Science, 2005: pp. 163–174. https://doi.org/10.3801/IAFSS.FSS.8-163.

[115] J. Burnford, D. Morrisset, A.O. Ojo, R.M. Hadden, A. Law, B. Peterson, Assessment and application of phosphor thermometry for spatially resolved surface temperature measurements during downward flame spread, Fuel 365 (2024). https://doi.org/10.1016/j.fuel.2024.131201.

[116] I. Vermesi, M.J. DiDomizio, F. Richter, E.J. Weckman, G. Rein, Pyrolysis and spontaneous ignition of wood under transient irradiation: Experiments and a-priori predictions, Fire Saf. J. 91 (2017) 218–225. https://doi.org/10.1016/j.firesaf.2017.03.081.

[117] E.T. Choong, F.O. Tesoro, F.G. Manwiller, Permeability of Twenty-Two Small Diameter Hardwoods Growing on Southern Pine Sites, 1974.

[118] D.N. Smith, E. Lee, The longitudinal permeability of some hardwoods and softwoods, HMSO, London, 1958.

[119] S. Lagüela, P. Bison, F. Peron, P. Romagnoni, Thermal conductivity measurements on wood materials with transient plane source technique, Thermochim. Acta 600 (2015) 45–51. https://doi.org/10.1016/j.tca.2014.11.021.

[120] H.P. Steinhagen, Thermal Conductive Properties of Wood, Green or Dry, from-40 deg to+ 100 deg C: A Literature Review., USDA Forest Serv Gen Tech Rep FPL-9 10 (1977).

[121] F. Yapici, A. Ozcifci, R. Esen, S. Kurt, Grain angle & thermal conductivity, 2011.

[122] ASTM E2058-13a, Standard Test Method for Measurement of Material Flammability Using a Fire Propagation Apparatus (FPA), 2013.

[123] D. Morrisset, S. Santamaria, R. Hadden, R. Emberley, Implications of data smoothing on experimental mass loss rates, Fire Saf. J. 131 (2022). https://doi.org/10.1016/j.firesaf.2022.103611.

[124] S.M. Dakka, G.S. Jackson, J.L. Torero, S.M. Mechanisms Dakka, Mechanisms Controlling the Degradation of Poly(methyl methacrylate) Prior to Piloted Ignition Proceedings of the Combustion Institute, 2002.

[125] R.J. Vyas, J.R. Welker, End-grain ignition of wood, The Journal of Fire & Flammability 6 (1976) 355–361.

[126] R. Bilbao, J.F. Mastral, M.E. Aldea, J. Ceamanos, M. Betrán, J.A. Lana, Experimental and theoretical study of the ignition and smoldering of wood including convective effects, Combust. Flame 126 (2001) 1363–1372. https://doi.org/10.1016/S0010-2180(01)00251-6.

[127] P.A. Beaulieu, N.A. Dembsey, Flammability characteristics at applied heat flux levels up to 200 kW/m2, Fire Mater. 32 (2008) 61–86. https://doi.org/10.1002/fam.948.

[128] M.B. Alam, S. Acharjee, S.M.A. Mahmud, J.A. Tania, M.M. Ali Khan, M.S. Islam, M.N. Khan, Household air pollution from cooking fuels and its association with under-five mortality in Bangladesh, Clin. Epidemiol. Glob. Health 17 (2022). https://doi.org/10.1016/j.cegh.2022.101134.

[129] J.R. Balmes, Household air pollution from domestic combustion of solid fuels and health, Journal of Allergy and Clinical Immunology 143 (2019) 1979–1987. https://doi.org/10.1016/j.jaci.2019.04.016.

[130] J.D. Mcdonald, B. Zielinska, E.M. Fujita, J.C. Sagebiel, J.C. Chow, J.G. Watson, Fine particle and gaseous emission rates from residential wood combustion, Environ. Sci. Technol. 34 (2000) 2080–2091. https://doi.org/10.1021/es9909632.

[131] N. MacCarty, D. Still, D. Ogle, Fuel use and emissions performance of fifty cooking stoves in the laboratory and related benchmarks of performance, Energy for Sustainable Development 14 (2010) 161–171. https://doi.org/10.1016/j.esd.2010.06.002.

[132] A.H. Mokdad, M.H. Forouzanfar, F. Daoud, A.A. Mokdad, C. El Bcheraoui, M. Moradi-Lakeh, H.H. Kyu, R.M. Barber, J. Wagner, K. Cercy, H. Kravitz, M. Coggeshall, A. Chew, K.F. O'Rourke, C. Steiner, M. Tuffaha, R. Charara, E.A. Al-Ghamdi, Y. Adi, R.A. Afifi, H. Alahmadi, F. AlBuhairan, N. Allen, M. AlMazroa, A.A. Al-Nehmi, Z. AlRayess, M. Arora, P. Azzopardi, C. Barroso, M. Basulaiman, Z.A. Bhutta, C. Bonell, C. Breinbauer, L. Degenhardt, D. Denno, J. Fang, A. Fatusi, A.B. Feigl, R. Kakuma, N. Karam, E. Kennedy, T.A.M. Khoja, F. Maalouf, C.M. Obermeyer, A. Mattoo, T. McGovern, Z.A. Memish, G.A. Mensah, V. Patel, S. Petroni, N. Reavley, D.R. Zertuche, M. Saeedi, J. Santelli, S.M. Sawyer, F. Ssewamala, K. Taiwo, M. Tantawy, R.M. Viner, J. Waldfogel, M.P. Zuñiga, M. Naghavi, H. Wang, T. Vos, A.D. Lopez, A.A. Al Rabeeah, G.C. Patton, C.J.L. Murray, Global burden of diseases, injuries, and risk factors for young people's health during 1990–2013: a systematic analysis for the Global Burden of Disease Study 2013, The Lancet 387 (2016) 2383–2401. https://doi.org/10.1016/S0140-6736(16)00648-6.

[133] G. Shen, K. Jiang, Substantial health threats from polluting household fuels, The Lancet 405 (2025) 1124–1125. https://doi.org/10.1016/S0140-6736(25)00467-2.

[134] N. García-López, A.S. Ingabire, R. Bailis, A.C. Eriksson, C. Isaxon, C. Boman, Biomass cookstove emissions—a systematic review on aerosol and particle properties of relevance

for health, climate, and the environment, Environmental Research Letters 20 (2025). https://doi.org/10.1088/1748-9326/adc615.

[135] J. Jetter, Y. Zhao, K.R. Smith, B. Khan, T. Yelverton, P. Decarlo, M.D. Hays, Pollutant emissions and energy efficiency under controlled conditions for household biomass cookstoves and implications for metrics useful in setting international test standards, Environ. Sci. Technol. 46 (2012) 10827–10834. https://doi.org/10.1021/es301693f.

[136] J.J. Flynn, R.M. Hadden, T.C. Bond, Particle measurements identify mechanisms in cold-start ignition of thermally-thick biomass – Submitted for publication, 2026.

[137] D. Morrisset, L. Schmidt, A. Law, R.M. Hadden, Carbon Monoxide and Carbon Dioxide Generation of Timber During Pyrolysis, Flaming, and Char Oxidation, in: 11th European Combustion Meeting, 2023.

APPENDIX

Supporting Information for Exploiting wood species and grain orientation to illuminate the onset of pyrolysis and ignition in deliberate combustion

John J. Flynn[a], David Morrisset[b], Rory M. Hadden[b], Tami C. Bond[a,1]

[a] Department of Mechanical Engineering, Walter Scott Jr. College of Engineering, Colorado State University, USA
[b] School of Engineering, The University of Edinburgh, U.K
1. Corresponding author

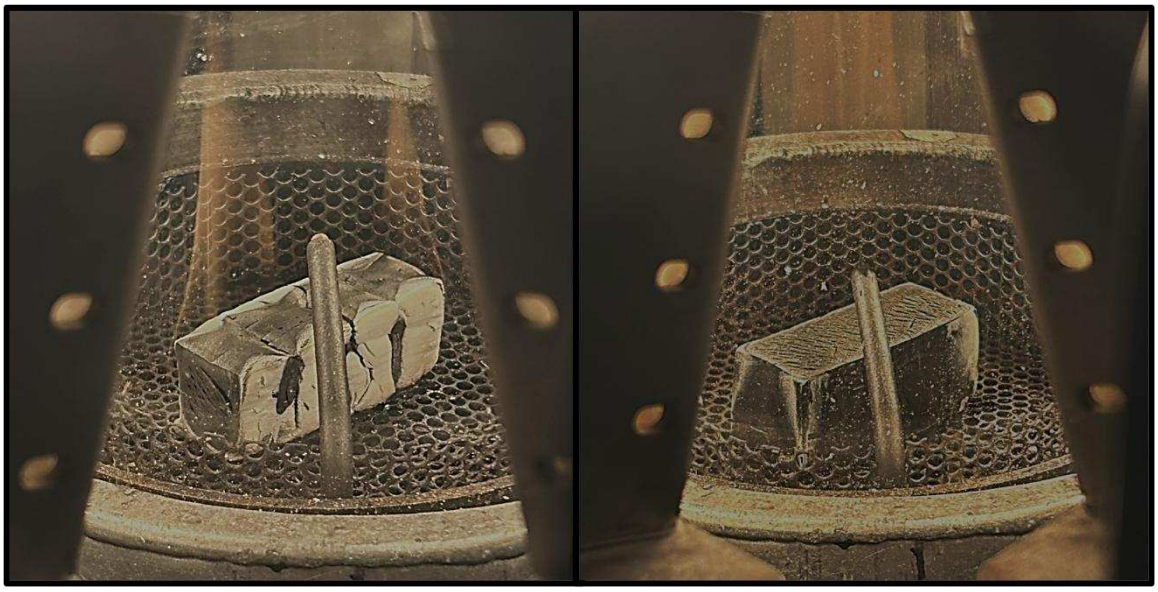

Figure S25. Photos showing flame formation from sample end grain in the *LGx* (left) and *LGz* (right) configurations at 40 kW m^{-2}. Photos were taken through a lens with high optical density to prevent damage to the camera.

Figure S25 photos show a sustained flame after ignition has occurred in the *LGx* and *LGz* configurations. The flame formed in the *LGx* orientation (left) is split into two conical flames which are localized at the ends of the sample. The flame formed in the *LGz* orientation (right) is a single conical flame which is evenly distributed along the heated surface of the sample. The photos show the visual effect of

fuel release from the end grain after ignition. This is consistent with the release of pyrolysis products. Flame photos are shown as pyrolysis products are less stable to photograph.

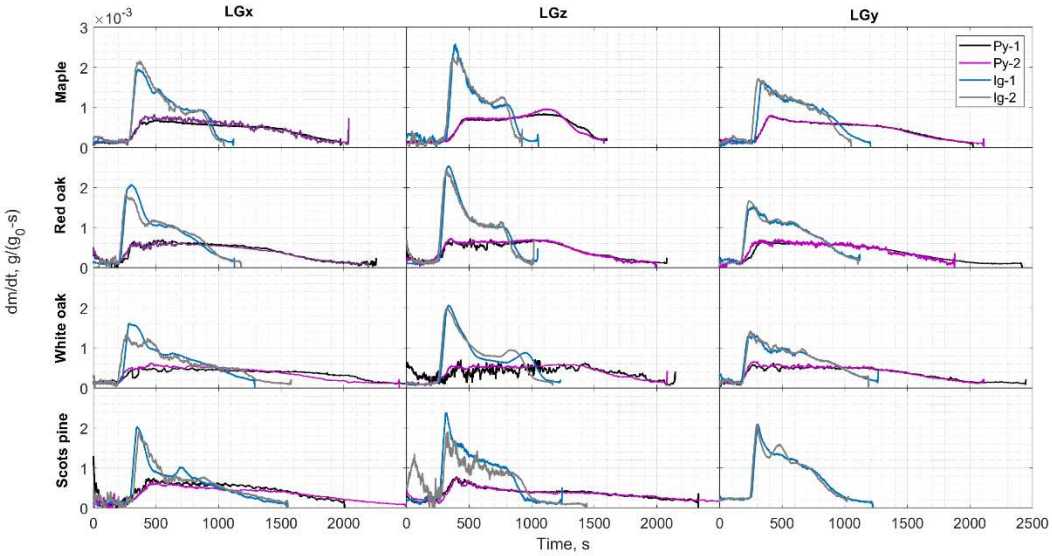

Figure S26. MLR profiles for all woods and configurations collected at 30 kW m^{-2}.

SI Table 4. Tabulated calculations used to determine ignition energy ratios for all conditions reported.

	30 kW/m2			
	Maple	**Red oak**	**White oak**	**Scots Pine**
Volume, m3	0.000063	0.000063	0.000063	0.000081
Density, kg/m3	705	700	755	520
Mass, kg	0.044415	0.0441	0.047565	0.04212
HF, kW/m2	30	30	30	30
Incident area, m2	0.0021	0.0021	0.0021	0.0027
Heat, kW	0.063	0.063	0.063	0.081
t_{ig}, *LGx*, s	285	209	212	303
Incident energy for ignition, kJ	18.0	13.2	13.4	24.5
t_{ig}, *LGy*, s	263	173	180	250
Incident energy for ignition, kJ	16.6	10.9	11.3	20.3
t_{ig}, *LGz*, s	309	256	256	271
Incident energy for ignition, kJ	19.5	16.1	16.1	22.0
Incident energy per unit mass, *LGx*, kJ/kg	404.3	298.6	280.8	582.7
Incident energy per unit mass, *LGy*, kJ/kg	373.0	247.1	238.4	480.8
Incident energy per unit mass, *LGz*, kJ/kg	438.3	365.7	339.1	521.2
Heat Value per unit mass, kJ/kg[a.]	18277.5	18765.7	18625.0	19945.7
IER[b.], *LGx*, kJ_consumed/kJ_released	0.0221	0.0159	0.0151	0.0292
IER[b.], *LGy*, kJ_consumed/kJ_released	0.0204	0.0132	0.0128	0.0241
IER[b.], *LGz*, kJ_consumed/kJ_released	0.0240	0.0195	0.0182	0.0261
Percent increase of *LGz* relative to *LGx*, %	8	22	21	-11
Percent increase of *LGy* relative to *LGx*, %	-8	-17	-15	-17

		40 kW/m2			
		Maple	**Red oak**	**White oak**	**Scots Pine**
Volume, m3		0.000063	0.000063	0.000063	0.000081
Density, kg/m3		705	700	755	520
Mass, kg		0.044415	0.0441	0.047565	0.04212
HF, kW/m2		40	40	40	40
Incident area, m2		0.0021	0.0021	0.0021	0.0027
Heat, kW		0.084	0.084	0.084	0.108
t_{ig}, *LGx*, s		123	93	90	137
Incident energy for ignition, kJ		10.3	7.8	7.6	14.8
t_{ig}, *LGy*, s		131	85	83	89
Incident energy for ignition, kJ		11.0	7.1	7.0	9.6
t_{ig}, *LGz*, s		162	121	127	119
Incident energy for ignition, kJ		13.6	10.2	10.7	12.9
Incident energy per unit mass, *LGx*, kJ/kg		232.6	177.1	158.9	351.3
Incident energy per unit mass, *LGy*, kJ/kg		247.8	161.9	146.6	228.2
Incident energy per unit mass, *LGz*, kJ/kg		306.4	230.5	224.3	305.1
Heat Value per unit mass, kJ/kg[a.]		18277.5	18765.7	18625.0	19945.7
IER[b.], *LGx*, kJ_consumed/kJ_released		0.0127	0.0094	0.0085	0.0176
IER[b.], *LGy*, kJ_consumed/kJ_released		0.0136	0.0086	0.0079	0.0114
IER[b.], *LGz*, kJ_consumed/kJ_released		0.0168	0.0123	0.0120	0.0153
Percent increase of *LGz* relative to *LGx*, %		32	30	41	-13
Percent increase of *LGy* relative to *LGx*, %		7	-9	-8	-35

Example Calculation:

Using an example trial of Maple wood at 30 kW/m^2 in the *LGx* grain orientation.

Determine volume of wood sample and use density to find sample mass.

$$V = depth, m\ x\ width, m\ x\ length, m\ [=]\ m^3$$

$$V = 0.03\ m\ x\ 0.03\ m\ x\ 0.07\ = 0.000063\ m^3$$

$$Density\ of\ maple\ (Table\ 1.)\ =\ 705\ kg/m^3$$

$$Mass = V,\ m^3\ x\ \rho_{Maple}, kg/m^3[=]\ kg$$

$$Mass = 0.000063\ m^3 x\ 705 \frac{kg}{m^3} = 0.0444\ kg$$

Determine incident heat on sample from FPA.

$$Incident\ area = 0.03\ m\ x\ 0.07\ m = 0.0021\ m^2$$

$$Incident\ heat\ on\ sample = 30 \frac{kW}{m^2} x\ 0.0021\ m^2 = 0.063\ kW$$

Determine how much incident heat on the sample up to the time of ignition:

$$t_{ig} = 285\ s$$

$$Incident\ energy\ for\ ignition = Incident\ heat\ on\ sample, kW\ x\ t_{ig}, s\ [=]\ kJ$$

$$Incident\ energy\ for\ ignition = 0.063\ kW\ x\ 285\ s = 18.0\ kJ$$

$$Incident\ energy\ per\ unit\ mass = \frac{Incident\ energy\ for\ ignition,}{Mass}$$

$$Incident\ energy\ for\ ignition\ per\ unit\ mass = \frac{18.0\ kJ}{0.0444\ kg} = 404.3\ kJ/kg$$

Heat value sourced from Phyllis data base. Numbers used are net calorific value (LHV) for dry wood.

$$Average\ Heat\ Value\ of\ Maple\ wood\ (LHV) per\ unit\ mass = \frac{[18.65 + 17.78 + 18.02 + 18.66] \frac{MJ}{kg}}{4}$$

$$= 18.2775 \frac{MJ}{kg}$$

$$Heat\ Value\ per\ unit\ mass = 18.2775 \frac{MJ}{kg} * 1000 \frac{kJ}{MJ} = 18277.5 \frac{kJ}{kg}$$

Determine ignition energy ratio by dividing incident energy for ignition by heating value of wood.

$$Ignition\ energy\ ratio\ (IER) = \frac{Incident\ energy\ for\ ignition\ per\ unit\ mass}{Heat\ Value\ per\ unit\ mass}$$

$$Ignition\ energy\ ratio\ (IER) = \frac{404.3\,\frac{kJ}{kg}}{18277.5\,\frac{kJ}{kg}} = 0.0221\ \ \frac{kJ\ Incident\ energy\ for\ ignition}{kJ\ Heat\ Value}$$

Example determination of percent change in *LGz* relative to *LGx*:

$$percent\ change = \frac{(0.0240 - 0.0221)}{0.0221} x\ 100 = 8.6\ \%$$